Received January 2, 2020, accepted February 4, 2020, date of publication February 10, 2020, date of current version March 12, 2020.

*Digital Object Identifier 10.1109/ACCESS.2020.2973130*

# Techno-Economic and Energy Efficiency Analysis of Optimal Power Supply Solutions for Green Cellular Base Stations

**ABU JAHID[1], (Student Member, IEEE), MD. SANWAR HOSSAIN[2], (Student Member, IEEE), MD. KAMRUL HASAN MONJU[3], MD. FAYZUR RAHMAN[4], AND MD. FARHAD HOSSAIN[5], (Member, IEEE)**

[1]Electrical and Computer Engineering, University of Ottawa, Ottawa, ON K1N 6N5, Canada
[2]Department of Electrical, Electronic and Communication Engineering, Military Institute of Science and Technology, Dhaka 1216, Bangladesh
[3]Department of Electrical and Electronic Engineering, Bangladesh University of Business and Technology, Dhaka 1216, Bangladesh
[4]Department of Electrical and Electronic Engineering, Green University of Bangladesh, Dhaka 1205, Bangladesh
[5]Department of Electrical and Electronic Engineering, Bangladesh University of Engineering and Technology, Dhaka 1205, Bangladesh

Corresponding author: Md. Sanwar Hossain (sanwareee@gmail.com)

This work was supported by the Faculty Research Fund of the Bangladesh University of Business and Technology.

**ABSTRACT** The widespread proliferation of internet access, affordable wireless gadgets, the user data demand and the corresponding extended cellular networks entailing significant energy consumption and carbon footprints. With the added benefits of renewable energy harvesting (REH) technology, telecom base stations (BSs) are predominantly supplied by green power sources to reduce operational expenditure (OPEX) and atmospheric pollution with guaranteed quality of service (QoS). Accordingly, this paper examines the plausibility of optimal power supply solutions such as standalone solar photovoltaic (PV), hybrid PV/wind turbine (PV/WT), hybrid PV/diesel generator (DG) and hybrid PV/electric grid (PV/EG) to feed the Long Term Evolution (LTE) BSs pertaining to technical, economic and environmental aspects in Bangladesh. An extensive Monte-Carlo based simulations are performed to evaluate wireless network performance in terms of throughput, energy efficiency (EE), energy efficiency gain ($EE_{gain}$), average energy savings, radio efficiency varying system bandwidth ($\mathcal{B}$) and BS transmission power ($P_{TX}$) considering the dynamic behavior of traffic intensity and renewable energy (RE) generation profile. By leveraging the cell zooming technique and a green traffic steering framework endeavors to minimize the net present cost and maximize the average energy savings as well. The simulation results reveal that the cell zooming technique attained energy savings yielding up to 36% and improvement of $EE_{gain}$ achieved about 23% with effective modeling of REH. Subsequently, a comprehensive comparison of the aforementioned schemes is pledged for further validation.

**INDEX TERMS** Green cellular networks, renewable energy harvesting, hybrid energy, energy efficiency, cell zooming, eco-sustainability, LTE.

## I. INTRODUCTION

Over the last few decades, the brisk expansion of mobile traffic and wireless multimedia services has driven to a remarkable enhancement of energy consumption in cellular communication. The evolution of mobile traffic demands such a video streaming service, cloud storage, and social networking is expected to increase the annual multiplication rate of 46% (i.e. a seven-fold increase) over the duration of 2016 to 2021 [1]. To tackle this escalating energy demand, telecom operators are deploying more BSs and leading to increasing a momentous portion of their capital expenditure (CAPEX) and OPEX accordingly. The tremendous expansion of cellular infrastructure leads to the mass consumption of non-renewable energy sources which causes an inconsistent rise of oil price and pollution to the environment. The heavy use of traditional energy supply imposes restrictions for network implementation in developing countries owing to the limited capability to carry the OPEX and related modern technologies. According to [2], the yearly energy expenditure for the cellular industry has uplifted from 219 TWh in 2007 to 354 TWh in 2012 across the worldwide. It has been estimated

The associate editor coordinating the review of this manuscript and approving it for publication was Giovanni Pau.

that worldwide energy consumption is prospective to increase about 37% from 2013 to 2035, or by an average of 1.4% annually and around 2-3% of global carbon content ejaculation is occurred by the information and communication technology (ICT) sector. Consequently, the electricity bill of telecom networks throughout the world amounts to above ten billion dollars per year and $CO_2$ emissions are also estimated to rise by a rate of 6% per year through 2020 [3]–[5].

Telecom equipment in the ICT circle is a major source of electricity consumption which is still expanding rapidly. According to [6], [7], BSs in the radio access networks (RAN) contribute about 60-80% of entire energy expenditure which places a cumbersome burden on the traditional grid supply and thereby contribute a significant amount of global carbon emissions to the atmosphere. Studies have revealed that paramount energy consumption in mobile networks is due to BSs which is typically designed for peak demand regardless of the tempo-spatial diversity of traffic load [8]–[10]. In response to the request of reducing energy consumption, dependency on conventional electric grid supply and importance on global development and financial aspects, cellular operators are extensively focused on green communications concentrating on minimum net present cost (NPC) and toxic emissions. Recently, access networks in green radio communication systems are widely supplied by sustainable, reliable, cost-effective and clean renewable energy sources (RES) that have drawn intense attention in both industry and academia [11]–[14]. For instance, Huawei [15] designed a solar PV energy-based 3G supported green cellular BSs in Bangladesh for reducing the sole dependency on-grid energy supply.

Typically, a diesel generator is often exploited to powering the remote cellular BSs where the electrical grid connection is not available or not suitable due to the geographical location [16]. The concept of deploying the diesel generator as the primary energy source has become much less viable from the economic perspective, technical issues and environmental implications. It is estimated that the greenhouse gas (GHG) outflow of the ICT sector will rise to 170 Mtons in 2014 to 235 Mtons by 2020, with 51% of $CO_2$ emissions generated by the telecom industry [17]. The burning of diesel fuel emits harmful components such as $CO_2$ significantly causes air pollution, raises the temperature of the world, and damages the ozone layer. Additionally, the reservation of fossil fuel is decreasing continuously and the cost of the fuel follows is in increasing nature. Furthermore, the lower efficiency and routine operation and maintenance (OMC) make the system much less reliable and resulting outage due to DG failure. Despite the numerous drawbacks of DG supply, a joint input supply technology (i.e. a combination of DG set or EG supply with green energy sources) offers an emergent solution in order to achieve reliability for the envisaged framework.

Being motivated from the aforementioned concerns, envisioning the future access networks to be powered by the standalone renewable energy sources and the conjunction of RES with the conventional energy sources are the excellent alternates in order to achieve a green cellular communication with a minimum amount of toxic carbon contents under low-cost electricity. Several studies [18]–[20] have carried out for curving down the energy costs by adopting standalone renewable energy sources to power cellular networks. Nonetheless, this could lead to a severe mismatch between load demand and interruptible RE supply, especially for large-scale wireless networks.

To address the intermittent, unreliable nature and dynamic variability of RE generation, envisioning the LTE BSs powered by diverse types of energy sources concurrently e.g., PV/WT, PV/DG, PV/EG has been recognized as a viable solution [21], [22] to save fossil fuel expenditure. The concept of jointly utilizing each BS with its individual energy harvester and storage devices offers some additional advantages together with the aforementioned ones such as it efficiently use the empty space and facilitates surplus electricity cooperation among surrounded BSs.

Cell zooming mechanism adaptively adjusts BS coverage depending on experienced traffic density and has the potential to reduce the energy consumption of an entire cellular network through balancing the traffic among surrounding BSs in a cluster [23]. Under zooming technology, a cell can extend its cell size based on low traffic demand and greater green energy availability, hence, cellular operators steer lower-traffic arrivals to its neighboring cell and thereby reduce overall consumption by turning off lightly loaded traffic cell. Energy efficiency is a key performance metric in green wireless communication to evaluate the network effectiveness which is directly related to aggregate throughput and net power consumption. Numerous studies have been performed focusing on throughput enhancement and EE assessment as well for next-generation green cellular infrastructure to explore the best solution [7], [23], [24]. This paper investigates energy efficiency analysis implementing a cell zooming technique for the optimal power supply option under a realistic scenario which offers an outstanding solution.

### A. CONTRIBUTIONS

The prime objective is carried out the optimization of RE utilization to minimize net present cost and fossil fuel consumption while ensuring long-term energy sustainability over a period of 20 years. The subsequent optimal techno-economic evaluation has been carried out for macro BS with remote radio head (RRH) unit ($N_{TRX} = 6$), omnidirectional ($N_{TRX} = 1$) configuration and microcell BS varying the system bandwidth and transmission power under a variety range of network settings. However, the optimization of technical and economic feasibility for various sorts of BS are analyzed using a hybrid optimization model for electric renewables (HOMER) software. Moreover, we formulate the various key performance metrics such as energy efficiency (EE), EE gain, energy consumption gain (ECG), radio efficiency ($\eta_{RE}$), throughput analysis to justify the effectiveness of the considered wireless network with different power supplies under optimal condition. Furthermore, the cell expanding concept is deployed to enhance EE. A comprehensive

Monte-Carlo based MATLAB simulation is used to measure the wireless network performance taking into consideration all factors. The key contributions of this manuscript can be summarized as follows.

- We investigate the feasibility of an adaptive power supply solution with an adequate energy storage device to power LTE cellular BSs based on resource readiness and BS types. The dimensioning of input power supply, energy-efficient mechanism to reduce non-renewable energy consumption, and optimization of the harvested green energy utilization for the considered framework are performed based on the minimization of the net system cost over 20 years' period maintaining sustainability issue.
- Particularly, we examined the multiple key implications: (i) the optimum size and technical criteria, (ii) energy breakdown analysis, (iii) cost evaluation, (iv) carbon emissions of standalone solar PV, hybrid PV/WT, hybrid PV/DG, and hybrid PV/EG power schemes considering the temporal fluctuation of solar/wind generation and dynamics of traffic arrival density under realistic network scenarios. To identifying best extent efficient power supply option, an extensive comparison is carried out by means of aforementioned metrics.
- A comprehensive Monte-Carlo based MATLAB simulations are conducted to assessment of wireless network performances in terms of different performance metrics such as energy efficiency, $EE_{gain}$, radio efficiency, energy consumption gain (ECG) in consideration of inter-cell interference (ICI) and shadow fading under a great variety of network settings. Thereafter, the average energy saving analysis has been carried out contemplated cell zooming technique with the considered hybrid-powered green cellular networks.

The rest of the paper is structured as follows. Relevant works are presented in section II. Section III represents the proposed system architecture along with solar PV model, WT model, fuel generator model, energy storage paradigm, load-dependent BS power model, formulation of performance metrics and cell zooming policy. Cost modeling and optimization problem formulation are presented in section IV. Section V demonstrates the simulation setup and the results analysis including optimal architecture, energy yield, cost analysis, and greenhouse gas emissions with insightful comments. In addition, wireless network performance evaluations are demonstrated in the same section. Section VI concludes the paper with key findings.

## II. RELATED WORKS

Recently, green cellular networking has drawn intensive attention from researchers and telecom operators owing to their financial and environmental advantages over a long period of time [25], [26]. Significant research works have been dedicated to optimizing the utilization of hybrid power supplies integration of RE enabled wireless networks aiming to investigate energy efficiency [27], improvement of throughput performance [23], network coverage [28], energy sharing strategy [3], still research in this field is not saturated yet. Authors proposed a new relay selection enabled power allocation technique to downsize the grid power consumption [29]. A user-BS association policy is adopted in [30] to enhance solar energy utilization. Authors did not focus on overall network throughput while offloading users' date rate through the networks. The aforementioned algorithms and solutions effectively balancing the traffic load, did not consider the optimal utilization of green energy as a key performance metric in the process of load balancing. Most of the mentioned studies pointed out either amplifying throughput, grid power minimization or adapting with network dynamics. Apart from this, the influence of minimum net present cost, optimal power supply solutions based on the geolocation together with energy efficiency analysis are crucial factors from the cellular operator's point of view are not investigated.

Alsharif *et. al.* [2], [13], [31] investigate the feasibility of off-grid power supply solutions for remote LTE BSs focusing on minimum net present cost without provisioning tempo-spatial variation of traffic intensity. In addition to this, wireless network performance and energy efficiency analysis is not considered in the paper. Authors [32] formulated a heuristic algorithm of solar PV assisted LTE macro BS for justifying minimum cost solution. Authors in [33] examined the feasibility of PV/DG/Battery hybrid power system based on combined dispatch control technology using HOMER. Moreover, techno-economic performance, overall cost, and environmental aspects are also investigated without consideration of the spatial diversity of solar production. The study of intermittent and unreliable nature of PV energy in Korea is counterbalanced by installing additional lithium-ion energy storage system including the cost analysis is carried out in [34]. Reference [35], [36] studies the prospects and challenges of solar and wind energy deployment in residential areas in terms of the energy production process, price, operation and maintenance cost, life span. Standalone green supply e.g. solar or wind power station is not a viable solution for designing a large scale zone uninterruptedly. Reference [37] computed power consumption scenario of HetNet LTE BSs implementing cell zooming mechanism without taking into account of actual traffic arrival rate and average energy savings for green cellular infrastructure. In this paper, we analyzed the best power supply solutions in a broader sense and compared them to other schemes for benchmarking.

Moreover, most of the authors have not analyzed the effective solution for LTE cellular networks under real-time traffic patterns. This approach may result in a huge dissipation of electricity during the low traffic period. Unlike the above techniques, a suitable user equipment (UE)-BS association policy based on downlink traffic arrivals can considerably reduce energy consumption by benefiting the capabilities of a number of RE enabled BSs. We approach the proper dimension of power supply solution ensuring desire sustainability for the envisaged green mobile networks to cope with the staggering rise of cellular traffic and diverse

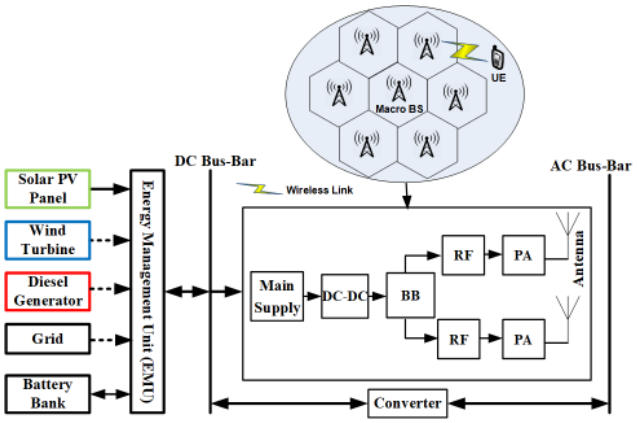


**FIGURE 1.** System architecture of the LTE macrocell BS.

applications varying bandwidth capacity under a wide range of context.

## III. SYSTEM MODEL

A single-tier downlink LTE cellular network having a set of $N$ geographically collocated BSs covering an area $\mathcal{A} = \{\mathcal{A}_1 \cup \mathcal{A}_2 \cup \ldots \cup \mathcal{A}_N\} \subset \mathbb{R}^2$ is considered. Here, $\mathcal{A}_i$ is the coverage area of BS $\mathcal{B}_i$, $\forall i \epsilon \{1, \ldots, N\}$. The system framework of the proposed LTE macrocell BS is shown in Fig. 1. The system layout can be classified into two types: input power supply unit and telecommunication load. In general, the BS consists of transceivers (TRXs) unit, power amplifiers (PAs) unit, a radio-frequency (RF) unit, a baseband (BB) unit, and a DC-DC power supply. The base station is powered by a standalone PV, hybrid PV/WT, hybrid PV/DG or hybrid PV/EG system with an energy storage device via an energy management unit (EMU). The EMU primarily uses the generated power from RES and distributes the excess energy according to the BS requirement. In addition, EMU is used to prevent the overvoltage and overcurrent which enhances the battery lifetime by limiting the intensive discharging of the storage device. Notably, PV array is primarily used to form aggregate supply either with WT, DG or EG sources since solar radiation intensity is proficient over the considered geographical region.

Note that locally available harvested green energy plays as primary power sources while non-RE sources e.g., DG or EG remain as a backup supply and BS consumes energy from a set of batteries in case of the deficiency of generation power. We consider different BS configurations namely 2/2/2 and omnidirectional arrangement in a hexagonal grid fashion with a RRH unit for LTE macro BS and micro BS. Modern cellular networks are widely adopted the concept of a distributed base station in which the BB signal processing unit is separated from radio frequency unit is defined as RRH. The base station with RRH provides a zero feeder loss due to the optical fiber link between the antenna and RF/PA components which allows higher system efficiency and provides a high level of flexibility. Moreover, no cooling arrangement is required in the RRH layout, thus significantly reduces overall

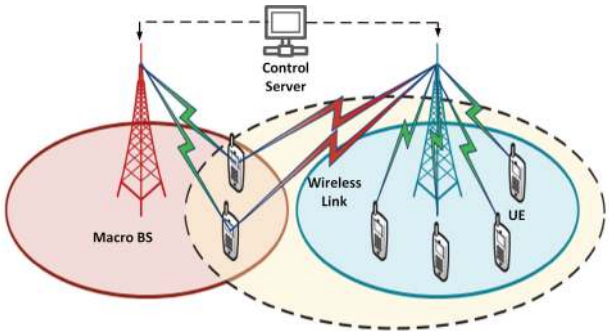


**FIGURE 2.** Traffic steering cell zooming model.

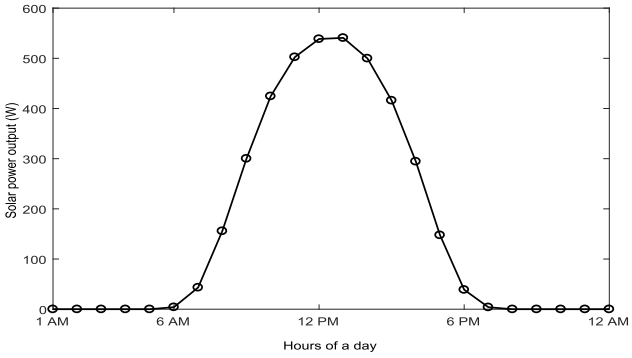


**FIGURE 3.** Average hourly solar power output for 1 kW PV array in a day.

energy consumption. The term 2/2/2 reflects a base station consists of three-sector with two antennas per sector. Fig. 2 depicts the concept of cell zooming technique where the red cell has a light load and shifts its associated users to the nearest surrounded BS. Furthermore, a control server is deployed in each cluster for monitoring the status of received signal power, traffic loads, energy availability to execute algorithms presented in section III-I aiming to maximize the EE.

### A. SOLAR PV PANEL

Multiple solar photovoltaic cells are connected in series/parallel to absorb sunlight and convert the naturally available plenty of solar energy into DC electrical energy to charge the battery bank and drive the telecom load. The solar PV power output is heavily affected by various factors such as the geographical position, solar PV panel rating, panel material, tilting of PV panel and the generation technology. Fig. 3 depicts the deviation of daily solar power production by 1 kW solar PV panel in the time domain, which is calculated with the help of the System Advisory Model (SAM). The annual DC electrical energy produced by the PV array can be measured using the following formula [13]

$$E_{PV} = C_{PV} \times \gamma_{avg} \times f_{PV} \times 365 day/year \quad (1)$$

where $C_{PV}$ denotes the solar PV panel rated capacity in kW, $\gamma_{avg}$ denotes the average daily solar irradiation in $kWh/m^2/day$ and $f_{PV}$ indicates the derating factor. Fig. 4 illustrates the solar resource profile over the one-year

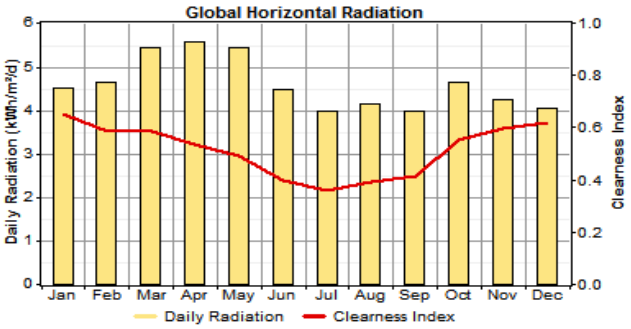


**FIGURE 4.** Average monthly solar irradiation index of Dhaka city.

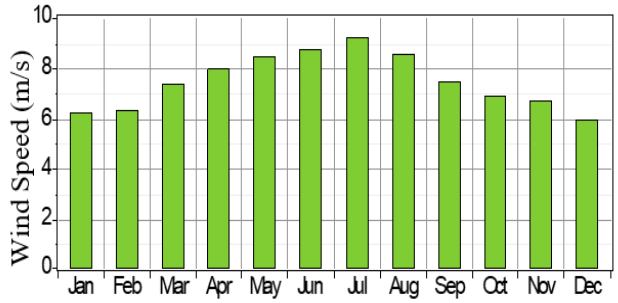


**FIGURE 5.** Average monthly wind speed for Patenga in Bangladesh [22].

duration in Dhaka city, Bangladesh. The yearly average solar radiation is 4.68 $kWh/m^2/day$ as obtained from Fig. 4.

### B. WIND GENERATOR

The wind generator is integrated with the solar PV panel in the coastal area or hill track region intending to ensure the sustainable and reliable power supply. A wind turbine generates electrical energy into two steps: first, it converts the wind power into mechanical energy and then transforms into electricity. The electrical power produced by WT mainly relies on wind velocity, weather system, and hub height. The amount of electrical power generated by the WT can be calculated by [13], [38]

$$P_{WT} = \frac{1}{2}\rho V_{avg}^3 C_p \tag{2}$$

where $V_{avg}$ is the average velocity of wind (m/s), $C_p$ is the coefficient of the Betz limit (typically 59% of maximum value), and $\rho$ is the monthly air density ($kg/m^3$). Typically, a Whisper 200 wind generator model is installed to powering cellular BSs due to low capital cost and longer life span [22]. Fig. 5 represents the monthly average wind velocity of Patenga city. The low solar power output during the rainy season is offset by the high power wind generation which leads to minimizing the fluctuation of hybrid RE production.

### C. DIESEL GENERATOR

Diesel generator (DG) plays a vital role when it is employed as a secondary power source unit during peak hours as it is not an attractive technology due to the lower efficiency. The integration of DG with the renewable energy sources can significantly meet the BS energy demand where RE is not sufficient. The high CAPEX of PV array is compensated by the low capital cost of the DG system, while the high operation & maintenance (OMC) cost of DG is counterbalanced by the low OMC of the PV system. The DG electricity production in a given rated power output ($P_{DG}$) is expressed as follows [39], [40]

$$E_{DG} = P_{DG} \times \eta_{DG} \times t_{eff} \qquad kWh \tag{3}$$

where $\eta_{DG}$ is the generator efficiency and $t_{eff}$ is the effective running hours. Additionally, the diesel consumption ($F_c$) in liter depends on the specific fuel consumption, $F_s(kWh)$ which is calculated as follows [40]

$$F_c = E_{DG} \times F_s \tag{4}$$

### D. BATTERY BANK

The battery bank is an energy storage device that enhances the power supply reliability providing backup supply during the absence or unpredictable fluctuation of RE generation. In this paper, the Trojan L16P lead-acid battery model has been selected due to improved capacity, small capital cost, high reliability, long-lasting and minimum maintenance. The selection of a battery cell unit is chosen based on the battery state of charge ($B_{SOC}$) condition and the nominal capacity.

The state of charge indicates the charging and discharging condition of the battery bank. $B_{SOC}$ is generally expressed in percentage, for instance, $B_{SOC} = 0\%$ represents that the full discharge state of the battery. On the other hand, $B_{SOC_{min}}$ indicates the lower threshold value of battery discharge and $B_{SOC_{max}}$ indicates the nominal capacity of the battery bank. Another important term battery bank depth of discharge which represents the peak energy be supplied from the storage that can be expressed as [13]

$$B_{DOD} = (1 - \frac{B_{SOC_{min}}}{100}) \tag{5}$$

Battery bank autonomy ($B_{aut}$) is one of the key factors that determine the potential number of hours and during this period the BS energy demand can be supplied by the battery bank without support from external energy sources. Battery bank autonomy is defined as the ratio of the entire storage size to the daily BS load [13]

$$B_{aut} = \frac{N_{batt} \times V_{nom} \times Q_{nom} \times B_{DOD} \times (24h/day)}{L_{BS}} \tag{6}$$

where $N_{batt}$ is the number of battery cells in the bank, $V_{nom}$ and $Q_{nom}$ is the nominal voltage (V) and the nominal capacity (Ah) of a single battery respectively and $L_{BS}$ is the average daily BS load in kWh.

Battery bank lifetime ($L_f$) is another fundamental issue that affects the replacement cost over the entire project. can be calculated using the following equation [13]

$$L_f = min(\frac{N_{batt} \times Q_{lifetime}}{Q_{thrpt}}, R_{batt,f}) \tag{7}$$

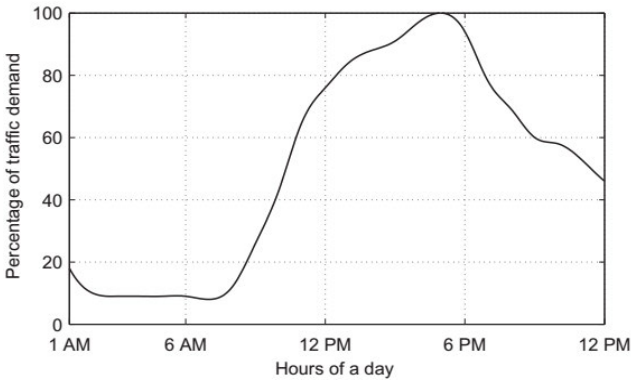


**FIGURE 6.** Traffic load profile in a day.

where $Q_{lifetime}$ is the lifetime throughput of a single battery (kWh), $Q_{thrpt}$ is the yearly energy output (kWh/year) and $R_{batt,f}$ is the battery float life (year).

### E. CONVERTER

A converter is used to convert the AC voltage into DC voltage (rectifier operation) or vice-versa (inverter operation). In this study, both the inverter and rectifier operation is implemented for supplying the AC load and DC load simultaneously. The capacity of the inverter mostly depends on the load demand and efficiency that can be calculated by the following equation [13]

$$C_{inv} = (\frac{L_{AC}}{\eta_{inv}}) \times S_f \tag{8}$$

where $L_{AC}$ represents the peak AC load in kW, $\eta_{inv}$ is the inverter efficiency, and $S_f$ is the safety factor.

### F. BS POWER CONSUMPTION MODEL

The efficient dimensioning of the sustainable power supply system is heavily affected by the BS load demand. In a practical cellular network, incoming traffic profile is time-varying and the load energy consumption is directly related to the traffic volumes. We consider the downlink traffic behaves in an inhomogeneous nature and is modeled using the Poisson distribution as shown in Fig. 6 [5].

$$\zeta(t) = \frac{p(t,\alpha)}{max[p(t,\alpha)]} \tag{9}$$

$$p(t,\alpha) = \frac{\alpha^t}{t!}e^{-\alpha} \tag{10}$$

where $\zeta(t)$ is the normalized traffic distribution, $p(t,\alpha)$ is the Poisson distribution function of traffic demand at a particular point of time, and is the mean value where the peak number of traffic arrivals occur at 5 PM.

Average traffic arrival intensity in $BS_i$ can be written as

$$\chi_i(t) = \lambda_i(t). \quad \rho_i(t). \quad \mu_{ik} \tag{11}$$

where $\lambda(t)$ presents arrival rate in time $t$, $\rho(t)$ service rate provided to users by $BS_i$, $\mu_{ik}$ is a binary decision variable and $U$ is the total number of users.

$$\mu_{ik} = \begin{cases} 1, & \text{if } UE_k \text{ is connected to } BS_i \\ 0, & \text{otherwise} \end{cases} \quad \forall i \epsilon \mathrm{N}, \forall k \epsilon \mathrm{U} \tag{12}$$

The total power consumption of a BS ($P_{BS}$) as a function of traffic intensity ($\chi$) and number of antennas can be represented as follows [41]

$$P_{BS} = \begin{cases} N_{TRX}[P_1 + \triangle_p P_{TX}(\chi - 1)], & \text{if } 0 < \chi \leq 1 \\ N_{TRX} P_{sleep}, & \text{if } \chi = 0 \end{cases} \tag{13}$$

where $P_1 = P_0 + \triangle_p P_{TX}$ is the maximum power consumption of a BS sector, $N_{TRX}$ is the total number of the transceiver indicates the total number of antennas in all three sectors, $\triangle_p$ is the load dependency power gradient and $P_0$ is the consumption at idle state. The scaling parameter $\chi$ is the load share, where $\chi = 1$ indicates a fully loaded system and $\chi = 0$ indicates an idle system. Furthermore, a BS without any traffic enters into sleep mode with low power consumption, $P_{sleep}$.

Power losses in BSs primarily occur in the DC-DC regulator ($\sigma_{DC}$), mains unit ($\sigma_{MS}$) and cooling system ($\sigma_{cool}$). Losses are linearly increasing with the power consumption of the other components. The maximum power consumption of the BS is calculated as

$$P_1 = \frac{P_{BB} + P_{RF} + P_{PA}}{(1-\sigma_{DC})(1-\sigma_{MS})(1-\sigma_{cool})} \tag{14}$$

$$P_1 = \frac{N_{TRX}\frac{\mathcal{B}}{10MHz}(P'_{BB} + P'_{RF}) + \frac{P_{TX}}{\eta_{PA}(1-\sigma_{feed})}}{(1-\sigma_{DC})(1-\sigma_{MS})(1-\sigma_{cool})} \tag{15}$$

where $P_{TX}$ is the BS transmission power in Watt and $\mathcal{B}$ is the transmission bandwidth in MHz. Also, $P'_{BB}$ and $P'_{RF}$ is the baseband and RF power consumption respectively.

The static consumption is independent of $\chi$ whereas the dynamic power consumption is varied with traffic loading parameter $\chi$ and the parameters for LTE BSs are summarized in Table 1.

The total energy consumption (calculated according to equation 13) of RRH enabled macro BS for two different configurations under 20W and 40W transmission power ($P_{TX}$) over a period of a day is presented in Fig. 7. Fig. 7 illustrates the variation of input power consumption with the system bandwidth demonstrating the impact of transmission power for traditional macrocell ($N_{TRX} = 6$) and omnidirectional architecture ($N_{TRX} = 1$). Notably, BSs power consumption is directly related to bandwidth as well as load demand and $P_{TX}$. According to the definition, the data presented in Fig. 7 follows a similar pattern to reach their peak values. According to the representation, higher bandwidth and $P_{TX}$ uplifts the BS power consumption regardless of the number of transceivers. It is obvious that a large amount of installed capacity is required to tackle cumbersome energy consumption while supporting tremendous traffic arrivals under the above provisions. However, microcell BS constitutes a total of 1126 W in a day according to (13) for particular settings.

**TABLE 1.** BS power model parameters for $\mathcal{B} = 10$ MHz at maximum load [10], [41].

| Parameters | Macro with RRH | Omnidirectional Macro RRH | Microcell |
|---|---|---|---|
| $P_{TX}$ [W] | 20 & 40 | 20 & 40 | 6.3 |
| $N_{TRX}$ | 6 | 1 | 2 |
| $\Delta_p$ | 2.8 | 2.8 | 2.6 |
| $P_0$ [W] | 84 | 84 | 56 |
| $P_{sleep}$ [W] | 56 | 56 | 39 |
| Feeder loss $\sigma_{feed}$ [dB] | 0 | 0 | 0 |
| PA efficiency $\eta_{PA}$ (%) | 31.1 | 31.1 | 22.8 |
| BB power $P'_{BB}$ [W] | 29.6 | 29.6 | 27.3 |
| RF Transceiver power $P'_{BB}$ [W] | 12.9 | 12.9 | 6.5 |
| PA power [W] | 64.4 | 64.4 | 27.7 |
| DC-DC $\sigma_{DC}$ (%) | 7.5 | 7 | 7.5 |
| Cooling $\sigma_{cool}$ (%)] | 0 | 0 | 0 |
| Main supply $\sigma_{MS}$ (%) | 9 | 9 | 9 |

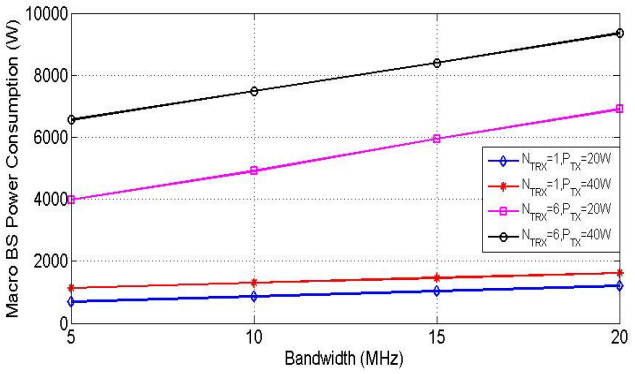


**FIGURE 7.** Daily BS load consumption for different bandwidth of macrocell.

A summary of notation symbols used in the algorithm section is presented in Table 2. The amount of remaining renewable energy $S(t)$ of $\mathcal{B}$ at time $t$ can be expressed as

$$S(t) = \epsilon S(t-1) + P_G(t) - P_{BS}(t) \tag{16}$$

where the storage factor $\epsilon$ identifies the percentage of energy leftover at the unit time $t$. For instance, $\epsilon = 0.95$ implies that 5% energy will be lost due to battery loss and converter loss. The stored energy in the battery bank should not grow bigger than maximum capacity. The surplus electricity ($E_{Excess}$) in kWh available at any BS can be defined as:

$$E_{Excess} = E_{in} - E_{BS} - L_{batt} - L_{cov} \tag{17}$$

where $L_{batt}$ and $L_{cov}$ represents the battery loss and converter loss respectively, $E_{BS}$ is the energy expenditure by each type of individual BS. $E_{in}$ denotes the total input power contribution which comprises of green power supply ($E_{RE}$) and non-renewable ($E_{NRE}$) sources such as DG set.

$$E_{in} = E_{RE} + E_{NRE} = E_{PV} + E_{WT} + E_{DG} \tag{18}$$

The quantity $E_{Excess}$ can be either positive or negative. Positive sign representing the cumulative input power entirely satisfy the networks load demand whereas negative quantity signifies a deficit of energy. In order to ensure guaranteed power reliability (i.e. zero outage), the installed capacity of input supply together with storage device is sufficient enough to meet demand under fully loaded condition without any energy wastage.

**TABLE 2.** Summary of the symbol notations.

| | |
|---|---|
| $\mathcal{RB}$ | Total number of resource block (RB) |
| $\mathcal{B}$ | Allocated bandwidth per RB |
| $\chi_{i,j}$ | Load demand of BS $\mathcal{B}_i$ at $j^{th}$ time |
| $N$ | Total number of LTE BSs |
| $P_{in}^{i,j}$ | Total input power for BS $\mathcal{B}_i$ in $j^{th}$ hour |
| $U$ | Total number of users |
| $P_G$ | Total green power generation |
| $S_p$ | Peak storage capacity |
| $S_{i,j}$ | Nominal storage capacity of $\mathcal{B}_i$ at $j^{th}$ time |
| $l_{k\forall N}$ | Path distance of $k^{th}$ UE from $N$ BSs |
| $SINR_{k\forall N}$ | SINR of $k^{th}$ user from $N$ BSs |
| $TP_j$ | Throughput for SINR based load balancing scheme |

### G. WIRELESS LINK REPRESENTATION

A log-normally distributed shadow fading wireless channel model is assumed in this study to calculate the signal to interference plus noise ratio (*SINR*). If $l$ is the separation distance (in $m$) between the base station and user, then the path-loss in dB can be expressed as

$$\gamma(l) = \gamma(l_0) + 10\delta log(\frac{l}{l_0}) + X_\sigma \tag{19}$$

where $\gamma(l_0)$ is the path-loss in dB at a near field reference distance $l_0$ and $\delta$ is the path-loss exponent. Path-loss can be calculated using the free-space Friss path-loss transmission formula and $X_\sigma$ is the amount of shadow fading modeled as a zero-mean Gaussian random variable with a standard deviation $\sigma$ dB.

The received power in dBm experienced by the for $k^{th}$ user equipment (UE) at a distance $l = l^{i,k}$ from $\mathcal{BS}_i$ is given by

$$P_r^{i,k} = P_t^{i,k} - \gamma(l) \tag{20}$$

The transmit power $P_t^{i,k}$ from $\mathcal{BS}_i$ to UE $k$ satisfies $\sum_{k\epsilon U} P_t^{i,k} \leq P_i^{max}$, where $P_i^{max}$ is RF output power its maximum traffic load.

The adjacent channel interference (ICI) and SINR can be expressed as:

$$P_{inter}^{i,k} = \sum_{m\neq i}(P_r^{m,k}) \tag{21}$$

$$SINR_{i,k} = \frac{P_r^{i,k}}{\mathcal{P}_{k,inter} + \mathcal{P}_{k,intra} + \mathcal{P}_N} \tag{22}$$

where $\mathcal{P}_{k,intra}$ is the intra-cell interference, $\mathcal{P}_N$ is the additive white Gaussian noise (AWGN) power given by $\mathcal{P}_N = -174 + 10log_{10}(\mathcal{B})$ in dBm with $\mathcal{B}$ is the bandwidth in Hz. Owing to the orthogonal frequency division multiple access (OFDMA) technique in LTE results in zero intra-cell interference. In addition, the inclusion of ICI from surrounded BSs is sufficient for calculating SINR in a regularly spaced hexagonal deployment scenario.

### H. PERFORMANCE METRICS

This section presents the formulation of different green metrics to validate the effectiveness of the proposed network. In this paper, the EE metric is defined as the ratio of total throughput (i.e. bit rate) in bit/sec to the overall fossil fuel-based power consumption. Total achievable throughput in a network can be calculated by Shanon's capacity formula as given below

$$TP_{tot} = \sum_{k=1}^{U}\sum_{i=1}^{N} \mathcal{B}log_2(1 + SINR_{i,k}), \text{ bps} \tag{23}$$

The EE metric denoted as $\eta_{EE}$ can be written as

$$\eta_{EE} = \frac{TP_{tot}}{P_{net}}, \quad \text{bits/joule} \tag{24}$$

where $P_{net} = \sum_{i=1}^{N} P_{BS}(i,t)$-$\sum_{i=1}^{N} P_G(i,t)$ is the net conventional energy consumption in BS $\mathcal{B}_i$ at time $t$, $P_{BS}(t)$ is the is the total input power in BS $\mathcal{B}_i$ at time $t$ and $P_G(t)$ is the green power utilized by the BS $\mathcal{B}_i$ BS at time $t$.

The metric EE gain ($EE_{gain}$) quantifies the level of improvement for the considered network performance with respect to the reference system. Energy consumption gain (ECG) is an equipment level metric measures the power required to transmit a single bit compared to the baseline reference scheme.

$$ECG = \frac{ECR_{Proposed}}{ECR_{Conventional}} \tag{25}$$

where the energy consumption ratio (ECR) is defined as the ratio of energy consumption to the system throughput given in Watt/bps.

**TABLE 3. UE-BS association policy for traffic steering load balancing algorithm.**

```
Initialize: RB, χ_{i,j}, χ_0, k ∈ 1, 2, ...U
for j = 1 : T
  for i = 1 : N
    if χ_{i,j} < χ_0 then
      Location of U = χ_{i,j} RB associated with B_i are updated
      for k = 1 : U
        Compute l_{k∀N} and SINR_{k∀N}
        Sort SINR_{k∀N} in descending order
          Associate k^{th} UE to the BS providing maximum SINR
          T_j = T_j + B log_2 (1+SINR_{i,k})
          Calculate average energy savings
          Update χ_{i,j}
        end for
    end if
  end for
end for
```

To the end, radio efficiency ($\eta_{RE}$) is a network level metric measure the spectral efficiency ($\eta_{SE}$) and coverage distance ($L$) attainable to the unit of power consumption.

$$\eta_{RE} = \frac{\eta_{SE} \times L}{P_{in}}, \quad \text{(bit.m)/sec/Hz/Watt} \tag{26}$$

### I. CELL ZOOMING ALGORITHM

This section presented different cell zooming algorithm, namely load balancing, green energy aware and the distance based setting goal is to reduction of energy consumption and improving of EE.

- Traffic steering load balancing: According to coordinated multipoint theory, a BS contributes highest SINR provides the best signal quality to users. Sort BSs in a cluster according to the traffic arrival intensity from low to high, corresponding load are $\chi_1, \chi_2, \chi_3, \ldots, \chi_N$. Set the load threshold $\chi_0$. If $\chi_{min} < \chi_0$, release the active BS of load $\chi_{min}$ and reallocate UE access. Check the user carrying capacity, then update transmission power and a new load set. Finally calculate energy consumption $P_{BS}$ and average energy savings. The Pseudo code of UE-BS connection policy under this category of cell zooming algorithm is presented in Table 3. Likewise, the algorithms for other two schemes can be illustrated in the similar way.
- Green energy aware: renewable energy generation exhibits tempo-spatial dynamics and each BS may experience different solar intensity depends on geographic location. Sort the BSs according to descending manner. Then, a top BS zooms out its coverage to support surrounding UEs whereas neighboring BSs zoom in to save more energy and may enter into sleep mode under 100% zoom out.

- Distance based: In a conventional scheme, the users will be connected with its closest BS. Sort BSs based on UE-BS distance in an ascending fashion. Set the threshold limit $l_{th}$, reduce transmission power as well as cell radius when $l < l_{th}$ and reallocate UEs. Determine the user interruption to the co-located BSs based on resource blocks and update entire $\chi$ of a network and $P_{TX}$. Calculate $P_{BS}$ and energy savings.

## IV. COST MODELLING AND PROBLEM FORMULATION

HOMER optimization tool is used to evaluate the optimal power supply system that satisfies user-specified constraints with the lowest net present cost ($NPC$) including the initial costs ($IC$), replacement costs ($RC$), operation and maintenance costs ($OMC$), and salvage value ($SV$) during the considered project lifetime. The $NPC$ of the system can be calculated by [13]

$$NPC = \frac{C_A}{F_{CR}} = IC + RC + OMC - SV \tag{27}$$

where total annualized cost ($C_A$) and capital recovery factor ($F_{CR}$) is given by (28) and (29) respectively [13].

$$C_A = C_{A.IC} + C_{A.RC} + C_{A.OMC} + C_{A.FC} \tag{28}$$

$$CRF = \frac{m(1+m)^D}{(1+m)^D - 1} \tag{29}$$

where $D$ represents the project duration (20 years) and $m$ indicates the annual interest rate.

The capital cost which remains at the end of the project lifetime is called salvage value [13]

$$SV = RC(\frac{L_{rem}}{L_{comp}}) \tag{30}$$

where $RC$, $L_{rem}$, and $L_{comp}$ are the replacement cost, remaining lifetime, and lifetime of the component respectively. For the DG and electric grid-enabled hybrid system, NPC also includes the fuel cost ($FC$). Hence $NPC$ can be determined as follows

$$NPC = IC + RC + OMC + FC - SV \tag{31}$$

The objective function of optimization is to minimize the $NPC$.

$$\text{minimize } NPC \tag{32a}$$

$$\text{subject to } E_{Gen} > E_{BS}, \tag{32b}$$

$$E_{Gen} + E_{batt} = E_{BS} + E_{losses}, \tag{32c}$$

$$E_{Excess} = E_{Gen} - E_{BS} - E_{losses}, \tag{32d}$$

$$E_{battmin} \leq E_{batt} \leq E_{battmax} \tag{32e}$$

where $E_{losses}$ comprises the annual battery loss and converter loss, $E_{BS}$ is the BS load consumption per year as obtained from Fig. 7 and $E_{batt}$ is the energy contribution from the storage device.

The constraint in (32b) validates that the yearly energy production for the proposed configuration carries the annual BS consumption. The aggregate energy contribution including battery supply satisfies the total energy consumption taken into two different losses is pointed out in constraint (32c). The amount of excess electricity is preserved for future use or in the abnormal condition is described by the constraint (32d). The constraint (32e) implies the storage capacity neither exceeds the maximum threshold limit and nor reached the below lower level.

**TABLE 4. HOMER simulation setup [5], [39], [42], [44].**

| System | Parameters | Value |
|---|---|---|
| Resources | $\gamma_{avg}$ | 4.68 kWh/$m^2$/day |
| | $V_{avg}$ | 7.48 m/s |
| | Annual interest rate | 6.75% |
| Solar PV | Operational lifetime | 25 years |
| | $\eta_{PV}$ | 0.9 |
| | System tracking | Two-axis |
| | $IC$ | \$1/Watt |
| | $RC$ | \$1/Watt |
| | $OMC$/year | \$0.01/Watt |
| Diesel Generator (DG) | $IC$ | \$0.66/Watt |
| | $RC$ | \$0.66/Watt |
| | $OMC$/year | \$0.05/hr |
| | Operational lifetime | 25,000hr |
| | Efficiency | 40% |
| Wind Turbine (WT) | Size | 1 kW |
| | Operational lifetime | 25 years |
| | Hub height | 10 m |
| | $IC$ | \$1.6/Watt |
| | $RC$ | \$1.6/Watt |
| | $OMC$/year | \$0.05/Watt |
| Electrical Grid (EG) | Energy price | \$0.120/kWhr |
| | Demand | \$0.350/kW/mo |
| Battery | Round trip efficiency | 85% |
| | $B_{SoC_{min}}$ | 30% |
| | $V_{nom}$ | 6 V |
| | $Q_{nom}$ | 360 Ah |
| | $Q_{lifetime}$ | 1075 kWh |
| | $IC$ | \$300/unit |
| | $RC$ | \$300/unit |
| | $OMC$/year | \$10/unit |
| Inverter | Efficiency | 95% |
| | Operational lifetime | 15 years |
| | $IC$ | \$0.4/Watt |
| | $RC$ | \$0.4/Watt |
| | $OMC$/year | \$0.01/Watt |

## V. PERFORMANCE ANALYSIS

### A. SIMULATION SETUP

In this section, we assume 20 years project lifetime and the yearly interest rate is 6.75% [42]. For ensuring the better quality of service, the annual capacity shortage has been selected to 0%. Moreover, dual-axis sun-tracking mode for PV panels is considered and 10% additional power is reserved to serve the BS load, even if the RE generation suddenly declines. HOMER makes a decision at each time step to satisfy the energy demand of BSs and keep provision for backup power at the lower net present cost. HOMER finds the optimal solution different sizes of solar PV, WT, DG, converter, and the number of batteries in from multiple iterations in the

**TABLE 5. Simulation parameters [43].**

| Parameters | Value |
|---|---|
| Resource block (RB) bandwidth | 180 kHz |
| System bandwidth, $\mathcal{B}$ (MHz) | 5, 10, 15, 20 |
| Carrier frequency, $f_c$ | 2 GHz |
| Duplex Mode | FDD |
| Cell radius | 1000 m |
| BS Transmission Power | 43 dBm & 46 dBm |
| Noise power density | -174 dBm/Hz |
| Reference distance, $l_0$ | 100m |
| Path loss exponent, $\delta$ | 3.574 |
| Shadow fading, $X_\sigma$ | 8 dB |
| Access technique, DL | OFDMA |

**TABLE 6. Zooming options for Macrocell [37].**

| Radius ($m$) | 400 | 600 | 800 | 1000 |
|---|---|---|---|---|
| Power radiated ($W$) | 17 | 25 | 33 | 40 |
| Zooming level (%) | 40 | 60 | 80 | 100 |

simulation process. Moreover, the cost parameters of different elements, duration of the lifecycle of each component, and the solar/wind profile of a particular area are set in the HOMER environment. Technical specifications, economic parameters and system constraints of the simulation setup are shown in Table 4.

Afterward, $\eta_{EE}$, throughput, $\eta_{RE}$, average energy savings, etc. performance metrics are evaluated using MATLAB for conduction network performance. Each data point is computed by averaging over 10000 iterations under the Monte-Carlo simulation. We assume uniform traffic distribution over the geographical region and each user occupies a single resource block (RB). A simulation setup according to 3GPP LTE standard [43] is presented in Table 5 whereas, Table 6 lists the zooming parameters for macro BS.

### *B. RESULT ANALYSIS*

This section emphasized several key features: (i) Optimal system design, (ii) Energy yield breakdown, (iii) Cost evaluation, (iv) GHG emissions and (v) Energy efficiency analysis. Additionally, relations of extended network sustainability and cost-effectiveness are thoroughly investigated and exhaustively analyzed with that of various parameters like system bandwidth ($\mathcal{B}$) and transmission power ($P_{TX}$).

#### 1) OPTIMAL SYSTEM DESIGN

The schematic diagram of optimal system architecture and load profile of LTE macro and micro BS under different settings in the HOMER platform are shown in Fig. 8 to Fig. 12. It is widely recognized that LTE macro BS operates at 20W (43dBm) and 40W (46dBm), but 20W transmit power is broadly used. On the other hand, microcell BS typically operates at 6.3W.

Table 7 and Table 8 summarizes the technical criteria of the system components for macrocell and microcell BS respectively under different transmission power and

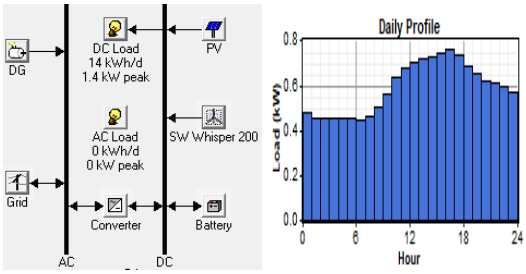


(a) Schematic layout (b) DC load

**FIGURE 8. Schematic layout and load profile of macrocell for $P_{TX} = 20$ W, $N_{TRX} = 6$, $\mathcal{B} = 10$ MHz.**

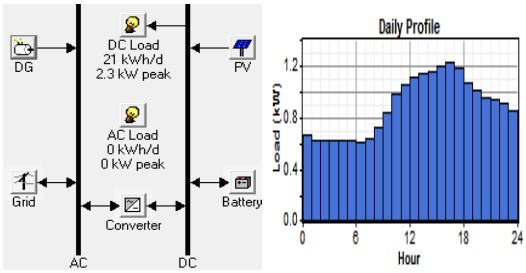


(a) Schematic layout (b) DC load

**FIGURE 9. Schematic layout and load profile of macro BS for $P_{TX} = 40$ W, $N_{TRX} = 6$, $\mathcal{B} = 10$ MHz.**

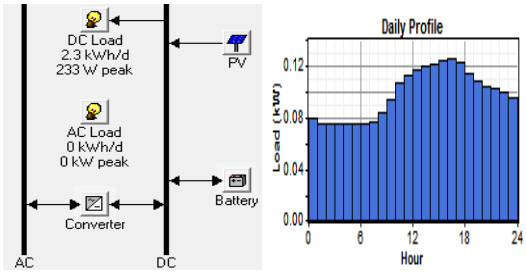


(a) Schematic layout (b) DC load

**FIGURE 10. Schematic layout and load profile of macro omnidirectional BS for $P_{TX} = 20$ W, $N_{TRX} = 1$, $\mathcal{B} = 10$ MHz.**

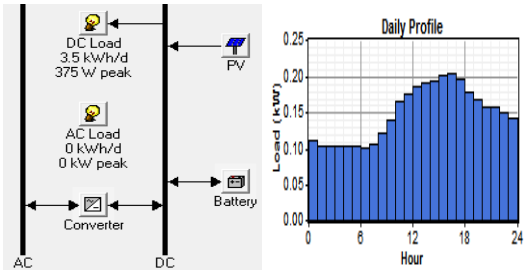


(a) Schematic layout (b) DC load

**FIGURE 11. Schematic layout and load profile of macrocell-omnidirectional for $P_{TX} = 40$ W, $N_{TRX} = 1$, $\mathcal{B} = 10$ MHz.**

**TABLE 7. Summary of optimum size for macro BS configuration with $\mathcal{B} = 10$MHz.**

| Components | $N_{TRX}$ | Standalone PV | | Hybrid PV/WT | | Hybrid PV/DG | | Hybrid PV/EG | |
|---|---|---|---|---|---|---|---|---|---|
| | | 20W | 40W | 20W | 40W | 20W | 40W | 20W | 40W |
| PV | 6 | 3 | 5 | 1.5 | 2.5 | 3.5 | 5.5 | 3 | 4 |
| (kW) | 1 | 1 | 1 | 0.1 | 0.1 | 1 | 1 | 0.2 | 1 |
| WT | 6 | - | - | 1 | 1 | - | - | - | - |
| (kW) | 1 | - | - | 1 | 1 | - | - | - | - |
| DG | 6 | - | - | - | - | 1 | 1 | - | - |
| (kW) | 1 | - | - | - | - | 1 | 1 | - | - |
| Converter | 6 | 0.01 | 0.01 | 0.01 | 0.01 | 0.01 | 0.01 | 0.01 | 0.02 |
| (kW) | 1 | 0.01 | 0.01 | 0.01 | 0.01 | 0.01 | 0.01 | 0.01 | 0.01 |
| Battery | 6 | 32 | 32 | 32 | 32 | 32 | 32 | 32 | 32 |
| (kW) | 1 | 32 | 32 | 32 | 32 | 32 | 32 | 32 | 32 |

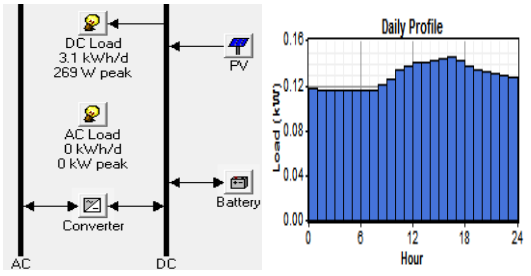


(a) Schematic layout (b) DC load

**FIGURE 12. Schematic layout and load profile of microcell for $N_{TRX} = 6.3$ W, $\mathcal{B} = 10$ MHz.**

**TABLE 8. Optimum components size for the microcell BS for different bandwidth.**

| $\mathcal{B}$ (MHz) | PV (kW) | Battery (units) | Converter (kW) |
|---|---|---|---|
| 5 | 1 | 32 | 0.01 |
| 10 | 1 | 32 | 0.01 |
| 15 | 1 | 32 | 0.01 |
| 20 | 1 | 32 | 0.01 |

bandwidth using HOMER simulation. As observed the number of the battery bank, converter, WT, and DG size remain constant for all network configurations which has a positive impact on supplying the BS energy demand. It is expected that micro BS requires smaller solar PV capacity as compared to the macro BS owing to low power expenditure. As seen, the optimal size of different components remains unchanged with respect to $\mathcal{B}$. Additionally, the dimension of the solar PV panel is follows increasing nature for the higher value of transmission power. This happens because higher $P_{TX}$ forces the BS energy demand to rise.

Fig. 13 represents the capacity of the solar PV panel ($C_{PV}$) for macro BS with RRH varying the transmission power and system bandwidth. The suggested network is simulated for different power supply solutions such as standalone solar PV, hybrid PV/WT, hybrid PV/DG, and hybrid PV/EG considering the average solar radiation profile ($\gamma_{avg}$) to find out the optimal system parameters. In this paper, solid lines indicate

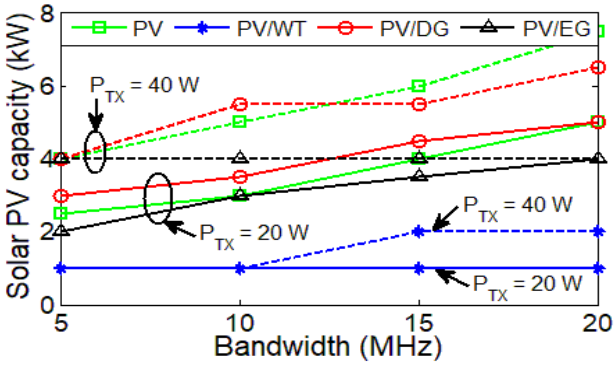


**FIGURE 13. Comparison of solar array size with $\mathcal{B}$ varying $P_{TX}$ for macro BS.**

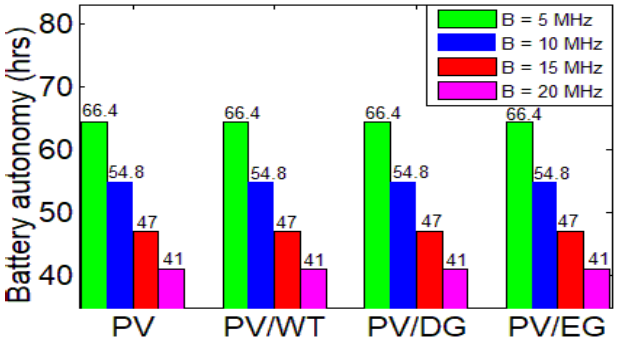


**FIGURE 14. Comparison of battery autonomy hours varying $\mathcal{B}$.**

the curve for $P_{TX} = 20$ W and the dashed line identifies the curve for $P_{TX} = 40$ W. It is observed that all curves following a gradual increment with the system bandwidth and $P_{TX}$. According to the denotation, large $\mathcal{B}$ and transmit power constitutes greater BS energy consumption which leads to the need for larger PV installed capacity. In other words, the linear rise of $C_{PV}$ capacity implies that the higher capacity PV panel is required to support BS load demand under higher $\mathcal{B}$ and $P_{TX}$. Finally, a greater value of PV array capacity has been found for hybrid PV/DG and standalone solar systems.

A thorough comparison of the battery bank autonomy ($B_{aut}$) for macrocell BS is shown in Fig. 14 and Fig. 15

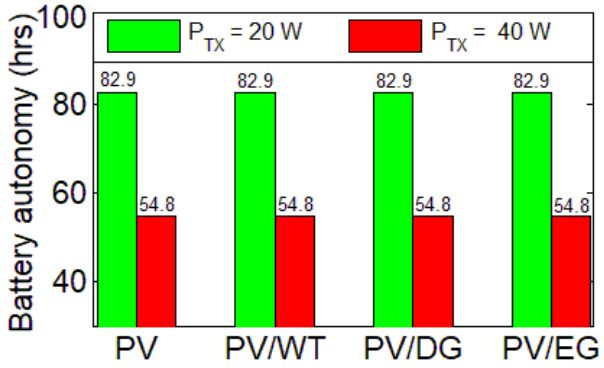


**FIGURE 15.** Variation of $B_{aut}$ varying transmission power for $\gamma_{avg}$ and $\mathcal{B} = 10$MHz.

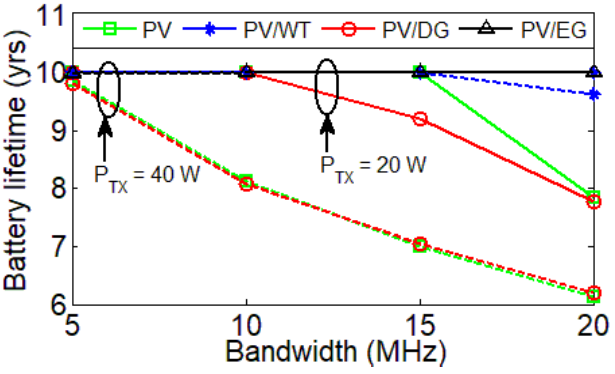


**FIGURE 16.** Battery bank lifetime comparison for $\gamma_{avg}$ varying $P_{TX}$.

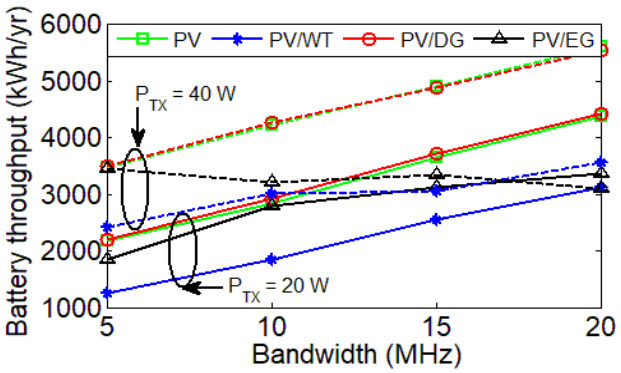


**FIGURE 17.** Battery throughput comparison of storage device for $\gamma_{avg}$ varying $P_{TX}$.

varying system bandwidth and $P_{TX}$ respectively. For ensuring the long term sustainability, a higher value of battery bank autonomy is preferable. However, $B_{aut}$ is inversely related to $\mathcal{B}$ and $P_{TX}$ as clearly seen from the figures. For example, the battery bank can independently feed BS demand more than 3 days under $\mathcal{B} = 10$ MHz during the absence of power supply which is enough time for maintenance. Moreover, a constant value of battery autonomy has been found for the standalone PV, hybrid PV/WT, hybrid PV/DG, and hybrid PV/EG powered system.

Fig. 16 and Fig. 17 represents the dependency of battery bank lifetime ($L_f$) and the battery throughput on the

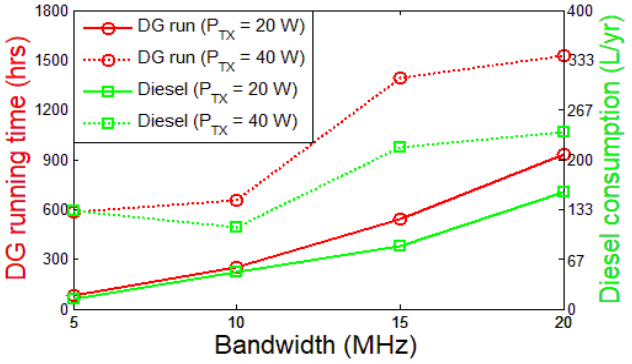


**FIGURE 18.** Comparison of DG operational time and diesel consumption.

bandwidth and transmit power for different power supply schemes. As seen, the annual throughput is a linear function of the system $\mathcal{B}$ regardless of the input supply mechanism. Meanwhile, a gradual decrement of $L_f$ is found for standalone solar PV and hybrid PV/DG system with the system bandwidth. On the other hand, $L_f$ remains nearly constant for hybrid PV/WT and hybrid PV/EG system. The state of battery bank energy level defines the throughput whereas the amount of stored energy that cycles in a year identifies the annual throughput ($Q_{thrpt}$). A higher $Q_{thrpt}$ is preferable for the considered network which is attained for the greater value of $\mathcal{B}$ as evident from the figure.

Fig. 18 expresses the detailed comparison of DG running time and annual diesel consumption with system $\mathcal{B}$ for different $P_{TX}$ of macro BS with RRH, $N_{TR} = 6$. Fig. 18 demonstrates that the DG operating time and fuel consumption curves follow a similar pattern of shifting upward direction corresponding to the system bandwidth. Notably, a higher DG operation hour enhance the fuel consumption and uplift the replacement cost as well as fuel cost. DG operational hours accompanied by its diesel consumption is comparatively higher for larger $P_{TX}$ owing to the increased load demand for the particular network setting.

### 2) ENERGY BREAKDOWN ANALYSIS

The annual energy generated by the PV array, wind turbine, and diesel generator along with a set of batteries based on the optimal design architecture has been critically discussed in this sub-section. Moreover, annual energy contribution, energy losses, and computation of excess electricity have been thoroughly evaluated under a different range of network parameters.

#### *a: SOLAR PV PANEL*

In this paper, Sharp ND-250QC solar module (polycrystalline) with a nominal voltage of 29.80 V, a nominal current of 8.40 A and power of 250 W is used for all network configuration. According to Table 7, solar PV array consists of 12 (i.e., 3 kW) and 20 (i.e., 5 kW) Sharp modules for standalone solar PV powered macro BS of 10 MHz bandwidth under 20 W and 40 W respectively. On the other hand, hybrid

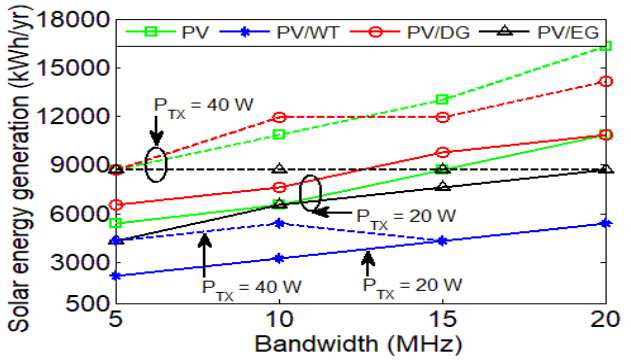


**FIGURE 19.** PV energy production with $\mathcal{B}$ varying $P_{TX}$ for different power supply schemes.

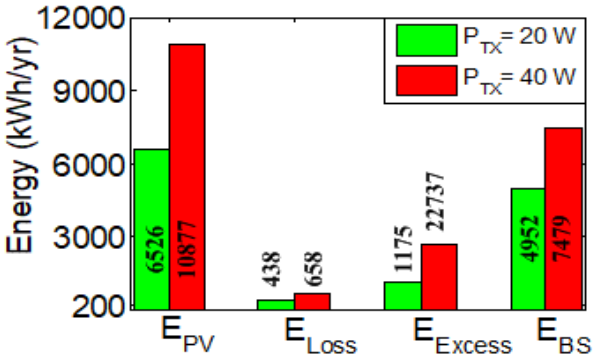


**FIGURE 20.** Annual energy breakdown for standalone solar PV macro BS.

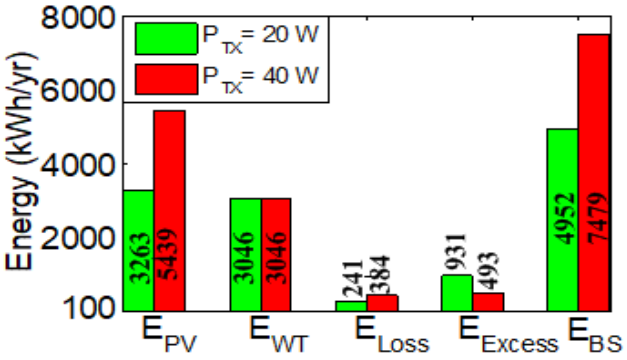


**FIGURE 21.** Annual energy breakdown for hybrid PV/WT macro BS.

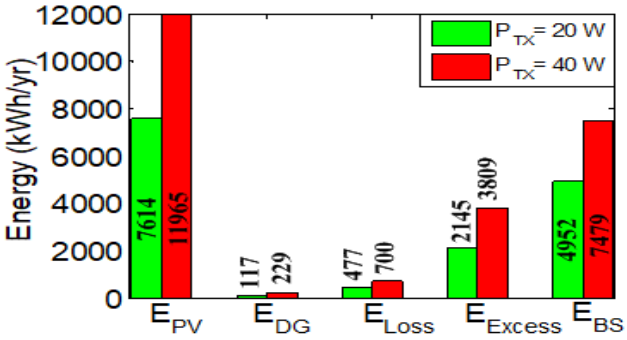


**FIGURE 22.** Annual energy breakdown for hybrid PV/DG macro BS.

PV/WT powered macro BS constitutes 6 (1.5 kW) and 10 (2.5 kW) solar PV panels for $P_{TX} = 43$dBm and 46dBm respectively. The yearly energy generation of 3 kW solar PV panel can be computed using equation (1); $E_{PV} = 3\ kW \times 4.68 \times 0.9 \times 365\ days/year = 4612$ kWh/year. However, a sun tracker mode increases the total amount of energy by 41% to be 6526 kWh/year. Similarly, the annual energy contribution of the 5 kW solar PV array is 10877 kWh. Likewise, solar energy production ($E_{PV}$) for micro BS can be determined using the optimal size obtained from Table 8.

Fig. 19 compares the annual PV energy generation with the bandwidth for the different power supply schemes. The network is simulated considering that each BS operates different bandwidth and transmit power to figure out an optimum component size under average solar radiation. Likewise, all curves follow an identical pattern to reach maximum value to meet up trending energy demand with the increment of $\mathcal{B}$ in Fig. 13. Moreover, higher PV production is found for the greater value of $P_{TX}$ as explained beforehand. In addition, $E_{PV}$ curves for $P_{TX} = 40$ W lies upper position over 20W condition due to the variation of load consumption.

### b: WIND TURBINE

The Whisper 200 model of 1 kW wind generator size connected to the DC bus-bar is a preferred choice for proposed networks under all considerations throughout this manuscript. The annual energy production from the WT is 3046 kWh used in HOMER simulation which is computed using (2).

### DIESEL GENERATOR

According to (3), 1 kW DG produces 117 kWh/year for $P_{TX} = 20$ W, $\mathcal{B} = 10$ MHz, ($P_{DG} = 1\ kW \times \eta_{DG} = 40\% \times t_{op} = 292.5$ hr/year) and 229 kWh/year for $P_{TX} = 40$W, $\mathcal{B} = 10$ MHz respectively for macro BS with RRH configuration.

### c: ENERGY BREAKDOWN

Fig. 20 to Fig. 23 summaries the annual energy comparison such as BS energy demand, energy loss, and excess electricity of the macro BS with $N_{TRX} = 6$ under the different power supply schemes (e.g., only solar PV, PV/WT, PV/DG, and PV/EG). The data presented in all figures have been derived for $P_{TX} = 20$ W and $P_{TX} = 40$ W for an average solar intensity ($\gamma_{avg}$) and 10 MHz bandwidth. In each iteration, HOMER calculates the losses ($E_{losses}$) comprising battery loss and converter loss and annual surplus electricity ($E_{Excess}$) which can be computed using equation (32d) for different configuration based on supplied energy. According to the illustrations, the upper value of $P_{TX}$ has a direct influence on BS energy consumption as well as energy generation, losses, and excess energy as explained beforehand. Note that a healthy amount of $E_{Excess}$ ensures a greater level of reliability during power sources malfunctioning or sudden disasters. It is observed that surplus electricity is comparatively much higher for standalone solar PV systems compared to that other

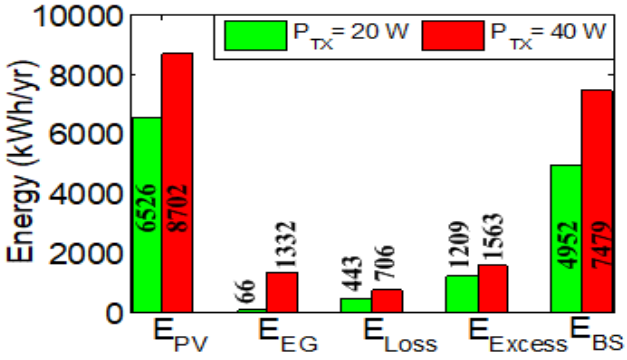


**FIGURE 23.** Annual energy breakdown for hybrid PV/EG powered macro BS.

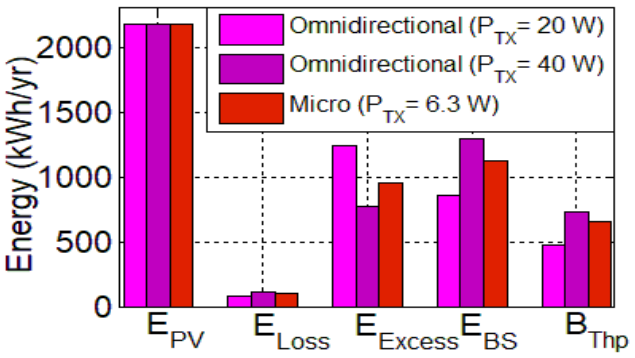


**FIGURE 24.** Annual energy breakdown for PV powered macro omnidirectonal and micro BS.

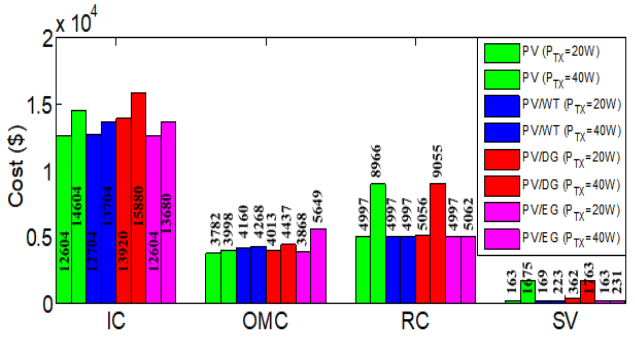


**FIGURE 25.** Cost comparison of macro BS for different power supply.

schemes because no other alternatives source exists if the PV supply fails.

The annual energy comparison of macro omnidirectional and micro BS with standalone solar PV supply is exhibited in Fig. 24 considering the average solar irradiation and 10 MHz system bandwidth. It is worthy to mention that the standalone solar PV powered scheme is sufficient to carry the macro BS with omnidirectional configuration and microcell BS load demand independently due to the smaller amount of energy requirement.

### 3) COST ANALYSIS

This subsection provides the details cost breakdown including the initial cost (*IC*), replacement cost (*RC*), operation & maintenance cost (*OMC*), salvage value (*SV*), fuel cost (*FC*) and net present cost (*NPC*) incurred within the project lifecycle.

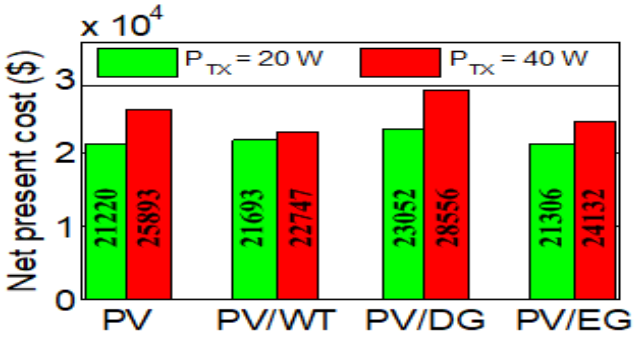


**FIGURE 26.** NPC comparison varying $P_{TX}$ for macrocell BS.

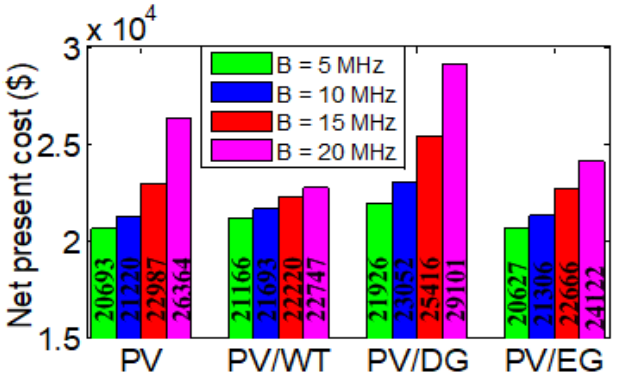


**FIGURE 27.** NPC comparison varying system bandwidth for macrocell BS.

The individual cost breakdown of various system components for the different supply schemes is illustrated in Fig. 25 considering the average solar intensity and 10 MHz bandwidth. The capital expense is directly related to the component size of the system which is paid at the starting of the project. On the other hand, *RC* is involved due to the lower life of the system components as compared to the project duration. However, a bulk amount of fuel cost is associated with diesel generator provision and partially in electric grid supply. In Bangladesh, the diesel price is $0.80 per liter [44]. Salvage value is the remaining cost of the components and estimated at the closing of the project duration. The NPC involves all costs that arise during the project duration which is computed using (27) every year.

Fig. 26 and Fig. 27 demonstrate the quantitative comparison of net present cost taking into account the effect of $P_{TX}$ and $\mathcal{B}$ respectively under the different power supply schemes. The graph depicts that high $P_{TX}$ and $\mathcal{B}$ incurs large *IC*, *OMC*, *RC*, and *NPC* likewise the results presented in the energy yield analysis section. It is also observed that the hybrid PV/DG powered system exhibits a higher *NPC* than the other power supply configurations. The hybrid PV/DG system involves a higher *OMC* and *FC* due to the continuous requirement of fossil fuel and the higher value of diesel price. The extensive use of DG running hours curtails the device

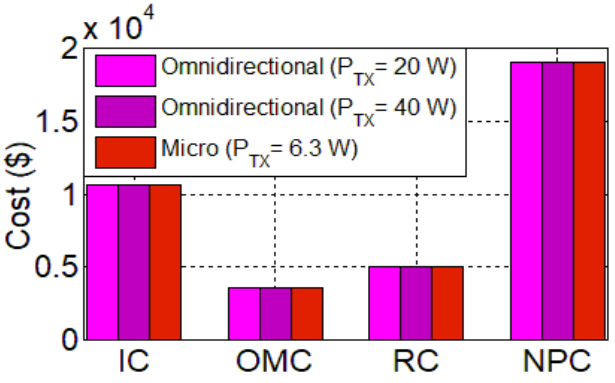


**FIGURE 28.** Comparison of cost analysis for macro omnidirectonal and micro BS under solar PV scheme.

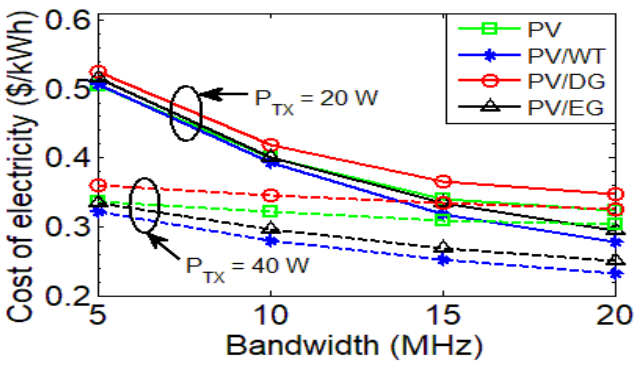


**FIGURE 29.** *COE* vs. $\mathcal{B}$ for different $P_{TX}$ under macro BS.

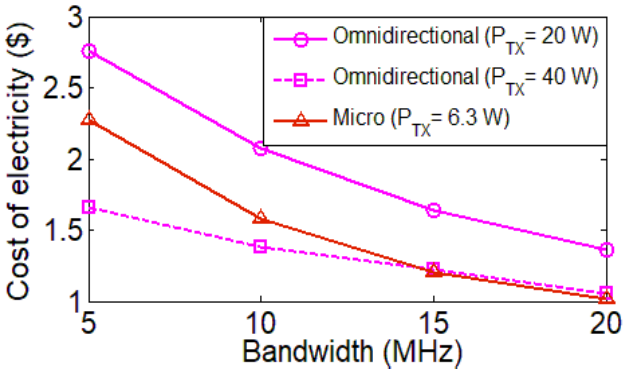


**FIGURE 30.** *COE* vs. $\mathcal{B}$ for different $P_{TX}$ under macro omnidirectional and micro BS.

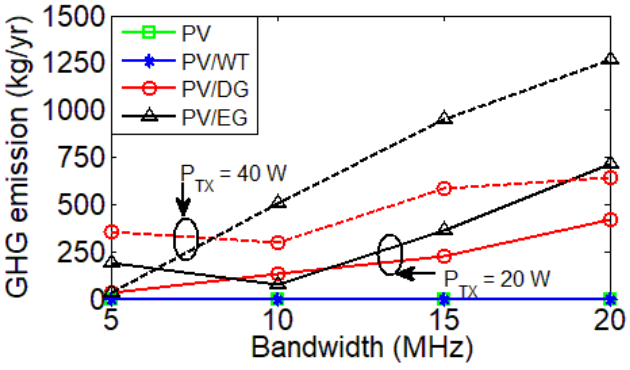


**FIGURE 31.** Comparison of carbon footprints for macro BS.

lifetime which causes the replacement cost also. *NPC* follows an increasing trend to cope up higher energy demand for the greater value of bandwidth as observed from Fig. 27. Standalone solar PV scheme shows superior *NPC* performance under all the cases as evident from Fig. 26 and Fig. 27. Finally, it can be concluded that higher $\mathcal{B}$ and $P_{TX}$ contributes a significant amount of NPC for the all supply arrangement and reduces the DG lifetime as well. In contrast, the lifecycle of PV/WT and PV/EG systems are independent of $\mathcal{B}$ and $P_{TX}$.

Fig. 28 represents the individual cost breakdown for the macro omnidirectional BS and microcell under 10 MHz bandwidth and $\gamma_{avg}$. It is noticed that NPC remains the same for omnidirectional 20 W, 40 W, and micro BS conditions because of insignificant change of an individual cost. This happens due to nearly equal energy demand which can be satisfied by the standalone solar PV system.

An extensive comparison of the cost of electricity (*COE*) under different power provisioning schemes for various $\mathcal{B}$ and $P_{TX}$ is illustrated in Fig. 29. It is observed that all the curves following a gradual decrement in nature with system $\mathcal{B}$ and higher $P_{TX}$, resulting in a lower per-unit electricity cost. It is also notable that the hybrid PV/DG scheme attains an inferior performance of *COE* whereas PV/WT provides an optimistic *COE* outcome compared to that of all the designated schemes under all cases.

Fig. 30 demonstrates the cost of electricity for omnidirectional macro BS and microcell BS with the system bandwidth. The *COE* curves for both configurations keeps up a similar trend to reach their minimum value which implies the inverse relationship to the system bandwidth. As seen, an augmented *COE* effectiveness is noticed for higher $\mathcal{B}$ and $P_{TX}$ whereas macro BS with $P_{TX} = 40$ W resembles the same result with micro BS for larger bandwidth.

### 4) GREENHOUSE GAS (GHG) EMISSIONS

Hybrid PV/DG and hybrid PV/EG scheme emit a significant amount of greenhouse gas due to the burning of fossil fuel for macro BS. A typical diesel generator emits around 2.68 kg of carbon content by burning one liter of diesel [40]. Fig. 31 manifests the comparison of greenhouse gas (GHG) emissions for aforementioned power supply schemes varying $P_{TX}$ with $\mathcal{B} = 10$ MHz. As expected, standalone PV and PV/WT produce zero carbon emissions whereas, PV/EG contributes a considerable amount of GHG ejaculation per year due to greater fuel consumption. The figure depicts that a higher system $\mathcal{B}$ and $P_{TX}$ contribute a greater amount of carbon pollutants to cope with up-trending BS demand. Results show that the dash line curve for $P_{TX} = 40$ W has a greater influence on carbon footprints over $P_{TX} = 20$ W owing to the deviation of load demand.

To the end, a standalone RE solution including adequate storage capacity is proposed for the low BS power profile such as microcell and macrocell with omnidirectional configuration due to the ubiquitous availability of solar

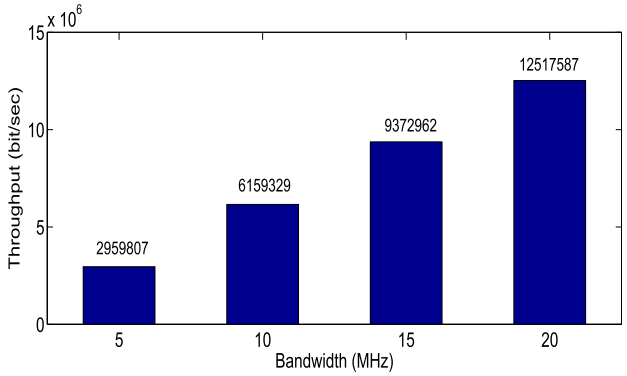


**FIGURE 32.** Throughput performance over a day for various $\mathcal{B}$.

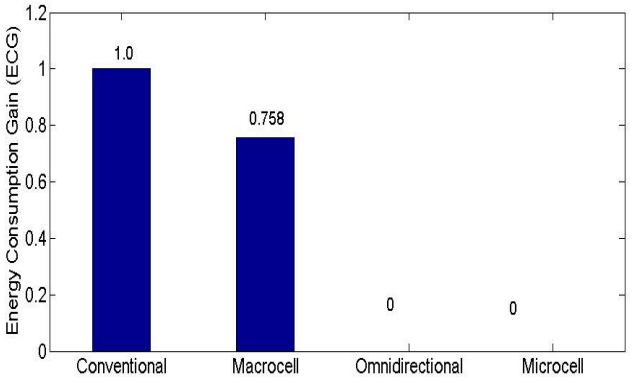


**FIGURE 33.** Variation of *ECG* for different BS configuration.

irradiation over the considered geographical area. On the other hand, a hybrid scheme is suggested for large-scale BS power expenditure (i.e. $N_{TRX} = 6$) based on resource availability. For instance, PV/WT power supply option is suggested near hill track or seashore regions where the wind is much available. Moreover, PV/DG/Battery aggregate solution can be implemented in remote areas where traditional grid supply is not available or involved immense installation cost and PV/EG/Battery hybrid supply is contemplated in urban or rural areas aiming to guaranteed eco-sustainability instead of using traditional EG/DG choice.

### 5) ENERGY EFFICIENCY ANALYSIS

In this section, the throughput performance, numerous types of performance metrics such as throughput, energy efficiency, energy efficiency gain, energy consumption gain (*ECG*), radio efficiency for the proposed network are clearly presented with insightful comments. In addition to this, the cell zooming technique is adopted to investigate the overall amount of savings and RE enhancement for the considered framework. It is worthy to mention that all the results presented under the network performance analysis section are simulated for average solar irradiation using Monte Carlo-based MATLAB simulation.

Throughput performance for the entire suggested network considering inter-cell interference over a period of a day is presented in Fig. 32. In LTE, the bit rate is directly related to the number of occupied resource blocks (RBs) i.e. active traffic. For instance, average traffic loading parameter at any time $t$, $\chi = 60\%$ signifies that 60% RBs are blocked. More specifically, 30 RBs are occupied while BSs operating on 10 MHz bandwidth and 20 RBs are kept reserved for taking further arrivals from neighboring BSs. It is worthy to mention that a large number of RBs are allocated while BS running in high $\mathcal{B}$. Therefore, throughput performance at $\mathcal{B} = 20$ MHz reveals an optimistic nature compared to others as evident from the figure.

Fig. 33 demonstrates a comparison of the *ECG* performance metric of various categories of BS type for the PV/DG power supply scheme with the conventional schemes. The term 'conventional' means the macrocell without RRH and solely run by fossil fuel-based energy sources. According to the definition of *ECG*, it measures the energy consumption improvement relative to the reference baseline system. It is observed that the proposed hybrid system with macro consumes about 24.21% less DG power compared to the conventional one whereas the amount of grid power consumed by microcell and omnidirectional layout is zero due to no fuel expenditure whatsoever.

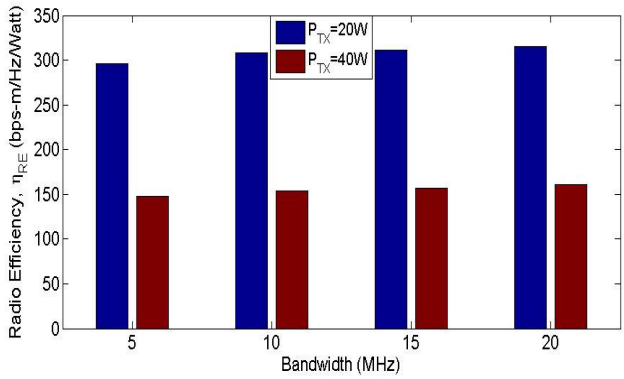


**FIGURE 34.** Comparison of radio efficiency varying $P_{TX}$ with $\mathcal{B}$.

Fig. 34 depicts the relation of throughput coverage per unit bandwidth and $P_{TX}$ for the considered cellular network. A gradual improvement of RE performance has been found for the higher system bandwidth. On the other hand, lower $P_{TX}$ uplifts $\eta_{RE}$ since $\eta_{RE}$ predominantly depends on spectral efficiency ($\eta_{SE}$) and $P_{in}$.

A comparison of EE performance metric for different input supply schemes varying $P_{TX}$ is illustrated in Fig. 35 considering tempo-spatial traffic arrival density ($\chi$). In accordance with denotation, $\eta_{EE}$ is directly related to the aggregate throughput and inversely varies with net power consumption. It is to be noted that throughput performance is varied with $\chi$ as well as resource blocks (RBs) whereas a higher bandwidth corresponds to a large number of RBs. As a consequence, a superior EE performance is observed for the higher RB allocation condition. On the other hand, the EE metric follows an upward direction for lower values of $P_{TX}$ as clearly observed from the figure. Additionally, the lower amount of grid or diesel energy consumption leads to prominent $\eta_{EE}$.

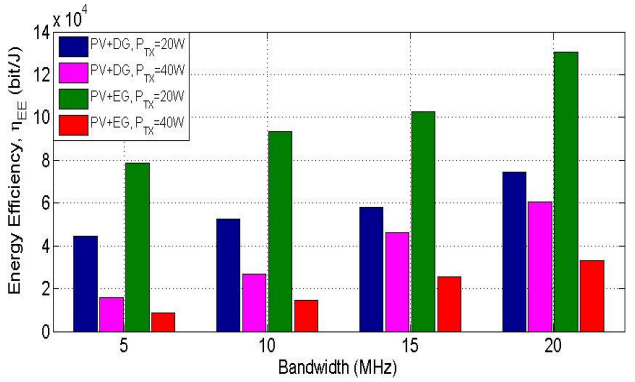


**FIGURE 35.** Comparison on EE performance of macrocell with bandwidth for various power supply schemes.

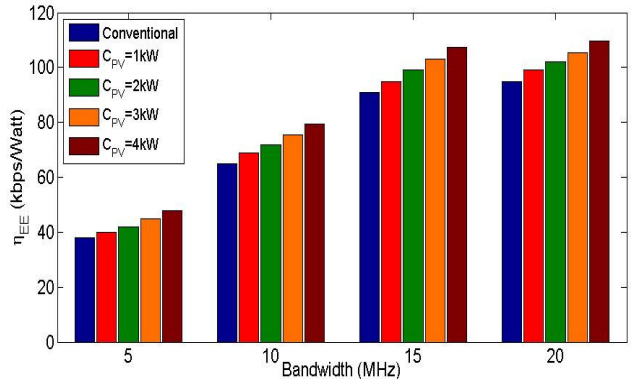


**FIGURE 36.** Quantitative EE performance comparison varying solar module capacity for PV/DG supply.

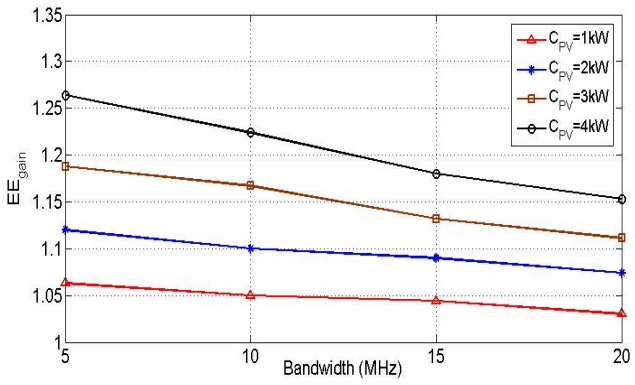


**FIGURE 37.** $EE_{gain}$ for the macro BS varying $C_{PV}$ with PV/DG supply.

In contrast, a comprehensive EE analysis is further carried out for different solar PV capacity with respect to $\mathcal{B}$ in Fig. 36. A greater value of solar energy generation decreases, leading to lower net conventional power consumption which eventually makes the zero fuel consumption state. With the help of the previous Fig. 35, the proposed framework keeps its optimistic trend with the system bandwidth and solar module capacity ($C_{PV}$) as well.

Fig. 37 illustrates the quantitative assessment of EE gain varying on-site installed solar harvester capacity for a particular network setup. $EE_{gain}$ measures the improvement of the

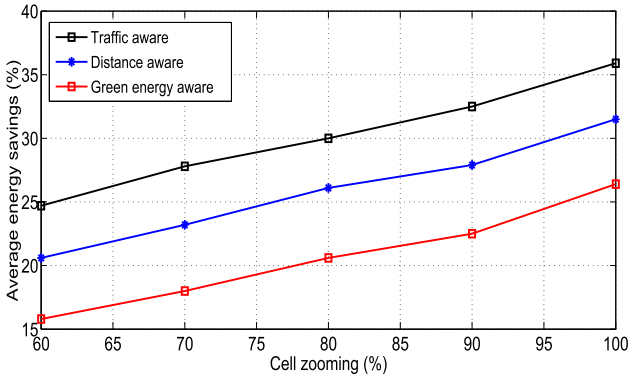


**FIGURE 38.** Average energy saving for different zooming techniques.

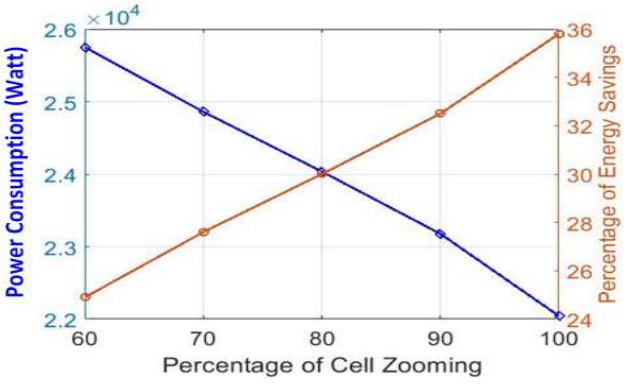


**FIGURE 39.** Average energy saving and power consumption scenario with cell zooming level.

considered network with respect to baseline scheme. In this paper, a LTE macro BS entirely run by PV/DG supply is contemplated as a reference baseline system. From the figure, higher solar output pushed EE gain in the up trending manner.

A detail comparison of three BS zooming options such as traffic aware, distance based and green energy availability is presented in Fig. 38. the traffic aware load balancing scheme keeps its optimistic nature achieving comparatively higher energy savings. Energy saving performance of the distance aware between UE and BS lies in between two other schemes as BS zooms out fluctuated over the arrival traffic load density. Notably, the energy saving performance follows similar fashion for all the three models due to the identical traffic variations. Further analysis of the figure identifies that traffic aware cell zooming technique attains 26.5% and 12% more energy savings performance over distance and green energy based mechanisms respectively.

Fig. 39 represents the percentage of average energy savings and overall power consumption in a day with the level of percentage of cell zooming for the considered macrocell BS. The concept of cell zooming is deployed for achieving higher EE performance during low traffic hours and peak solar energy generation period. For the sake of simplicity, one cell lies in the center of first cellular tier is assumed for different level of cell zooming based on the traffic demand and PV production. As seen, the energy savings is linearly scaled up to 36% with

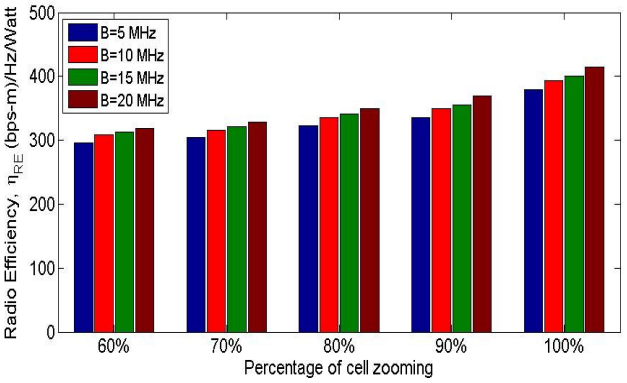


**FIGURE 40.** Radio efficiency vs percentage of cell zooming.

cell zooming factor guaranteeing remarkable EE performance without zero outage. However, the net power consumption of the entire cellular network demonstrate the opposite trend with the increment of zooming level. Note that 70% cell zooming implies that the neighboring cells contribute 30% of coverage and goes into sleep mode, thereby saves a substantial amount of energy. It is important to mention that the sleeping cell must switch on without sacrificing the entire system performance.

Fig. 40 is derived with the help of Fig. 34 and Fig. 39 to represent the $\eta_{RE}$ with the percentage of cell zooming for different system bandwidth. The upward trending nature of $\eta_{RE}$ implies the relatively higher network improvement with the increment of zooming level and $\mathcal{B}$ as evident from the figure. Therefore, it can be readily concluded that the hybrid power supply scheme with a cell zooming mechanism for the macro BS attains the maximum energy efficiency under the optimal condition with guaranteed QoS.

## VI. CONCLUSION

This paper addresses the effectiveness of LTE macro/micro base stations at off-grid/on-grid sites in Bangladesh provisioned to be powered by the standalone solar PV, hybrid PV/WT, hybrid PV/DG, and hybrid PV/EG scheme. The techno-economic analysis together with environmental aspect have been extensively evaluated in accordance with optimal system architecture. For benchmarking, the performance of different power supply schemes have been thoroughly analysed varying the system bandwidth and transmission power. From the simulation results, a continuous improvement of NPC and the cost of electricity has been found for a higher value of $\mathcal{B}$ and $P_{TX}$. The numerical results reveal that the hybrid PV/WT scheme is an excellent solution for powering the macro BS as it provides a lower value of *COE* and zero GHG, but WT is not feasible in all areas. On the other hand, standalone solar PV system provides an attractive alternative for powering both macro with omnidirectional layout and micro BS around all the location since this scheme contributes zero carbon emissions with minimum NPC which has a positive impact of per unit electricity generation cost also. Additionally, surplus energy production ensures a greater level of reliability in the long run without any help from external retailers. Moreover, the battery bank backup can feed the LTE macro BS for 82.9 hours ($P_{TX} = 20$ W) and 54.8 hours ($P_{TX} = 40$ W) autonomously if the hybrid PV/WT system fails to support the BS energy demand. On the other hand, integration of cell zooming technique under optimal condition outperforms a lot better in terms of energy efficiency, radio efficiency and average grid energy savings and thereby makes the system more lucrative. However, three cell zooming algorithms are widely compared to find best extent efficient options in terms of energy savings in where results revealed that load balancing traffic aware scheme more efficient yielding up to 26.5% and 12% over distance based and green energy aware mechanisms respectively. Further extension will focus on developing coordination and relay based generalized algorithm for heterogeneous networks.

**Conflicts of Interest**: The authors declare that they have no conflict of interest.

## ACKNOWLEDGMENT

This work was supported by the Faculty Research Fund of the Bangladesh University of Business and Technology.

## REFERENCES

[1] L. A. Fletscher, L. A. Suarez, D. Grace, C. V. Peroni, and J. M. Maestre, "Energy-aware resource management in heterogeneous cellular networks with hybrid energy sources," *IEEE Trans. Netw. Service Manage.*, vol. 16, no. 1, pp. 279–293, Mar. 2019.

[2] M. H. Alsharif, "Techno-economic evaluation of a stand-alone power system based on solar power/batteries for global system for mobile communications base stations," *Energies*, vol. 10, no. 3, p. 392, Mar. 2017.

[3] M. J. Farooq, H. Ghazzai, A. Kadri, H. ElSawy, and M.-S. Alouini, "A hybrid energy sharing framework for green cellular networks," *IEEE Trans. Commun.*, vol. 65, no. 2, pp. 918–934, Feb. 2017.

[4] F. Ahmed, M. Naeem, and M. Iqbal, "ICT and renewable energy: A way forward to the next generation telecom base stations," *Telecommun. Syst.*, vol. 64, no. 1, pp. 43–56, Mar. 2016.

[5] A. Jahid, M. K. H. Monju, M. E. Hossain, and M. F. Hossain, "Renewable energy assisted cost aware sustainable off-grid base stations with energy cooperation," *IEEE Access*, vol. 6, pp. 60900–60920, 2018.

[6] M. Ismail, W. Zhuang, E. Serpedin, and K. Qaraqe, "A survey on green mobile networking: From the perspectives of network operators and mobile users," *IEEE Commun. Surveys Tutr.*, vol. 17, no. 3, pp. 1535–1556, 3rd Quart., 2015.

[7] A. Jahid, K. H. Monju, S. Hossain, and F. Hossain, "Hybrid power supply solutions for off-grid green wireless networks," *Int. J. Green Energy*, vol. 16, no. 1, pp. 12–33, Oct. 2018.

[8] M. A. Safwat, "Framework for multi-operator collaboration for green communication," *IEEE Access*, vol. 6, pp. 850–865, 2018.

[9] A. M. Aris and B. Shabani, "Sustainable power supply solutions for off-grid base stations," *Energies*, vol. 8, no. 10, pp. 10904–10941, Sep. 2015.

[10] A. Jahid and S. Hossain, "Intelligent energy cooperation framework for green cellular base stations," in *Proc. Int. Conf. Comput., Commun., Chem., Mater. Electron. Eng. (IC4ME2)*, Feb. 2018, pp. 1–6.

[11] A. S. Aziz, M. F. N. bin Tajuddin, and M. R. bin Adzman, "Feasibility analysis of PV/wind/battery hybrid power generation: A case study," *Int. J. Renew. Energy Res.*, vol. 8, no. 2, pp. 661–671, Jun. 2018.

[12] P. Gandotra, R. K. Jha, and S. Jain, "Green communication in next generation cellular networks: A survey," *IEEE Access*, vol. 5, pp. 11727–11758, 2017.

[13] M. Alsharif and J. Kim, "Hybrid off-grid SPV/WTG power system for remote cellular base stations towards green and sustainable cellular networks in South Korea," *Energies*, vol. 10, no. 1, p. 9, Dec. 2016.

[14] A. Jahid and S. Hossain, "Dimensioning of zero grid electricity cellular networking with solar powered off-grid BS," in *Proc. 2nd Int. Conf. Electr. Electron. Eng. (ICEEE)*, Dec. 2017, pp. 1–4.
[15] Huawei. *Mobile Networks go Green*. Accessed: Nov. 30, 2019. [Online]. Available:http://www.huawei.com/en/abouthuawei/publications/communicaite/hw- 082734.htm
[16] A. Jahid, M. S. Islam, M. S. Hossain, M. E. Hossain, M. K. H. Monju, and M. F. Hossain, "Toward energy efficiency aware renewable energy management in green cellular networks with joint coordination," *IEEE Access*, vol. 7, pp. 75782–75797, 2019.
[17] V. Chamola and B. Sikdar, "Solar powered cellular base stations: Current scenario, issues and proposed solutions," *IEEE Commun. Mag.*, vol. 54, no. 5, pp. 108–114, May 2016.
[18] P.-H. Chiang, R. B. Guruprasad, and S. Dey, "Optimal use of harvested solar, hybrid storage and base station resources for green cellular networks," *IEEE Trans. Green Commun. Netw.*, vol. 2, no. 3, pp. 707–720, Sep. 2018.
[19] A. Jahid, A. B. Shams, and M. F. Hossain, "Green energy driven cellular networks with JT CoMP technique," *Phys. Commun.*, vol. 28, pp. 58–68, Jun. 2018.
[20] J. Leithon, T. J. Lim, and S. Sun, "Cost-aware renewable energy management with application in cellular networks," *IEEE Trans. Green Commun. Netw.*, vol. 2, no. 1, pp. 316–326, Mar. 2018.
[21] D. Renga and M. Meo, "Dimensioning renewable energy systems to power mobile networks," *IEEE Trans. Green Commun. Netw.*, vol. 3, no. 2, pp. 366–380, Jun. 2019.
[22] M. S. Hossain, A. Jahid, and M. F. Rahman, "Quantifying potential of hybrid PV/WT power supplies for off-grid LTE base station," in *Proc. Int. Conf. Comput., Commun., Chem., Mater. Electron. Eng.*, Rajshahi, Bangladesh, Feb. 2018, pp. 1–5.
[23] B. Xu, Y. Chen, J. Requena Carrion, J. Loo, and A. Vinel, "Energy-aware power control in energy cooperation aided millimeter wave cellular networks with renewable energy resources," *IEEE Access*, vol. 5, pp. 432–442, 2017.
[24] A. Bin Shams, A. Jahid, and M. F. Hossain, "A CoMP based LTE–A simulator for green communications," in *Proc. Int. Conf. Wireless Commun., Signal Process. Netw. (WiSPNET)*, Mar. 2017, pp. 1751–1756.
[25] F. Ahmed, M. Naeem, W. Ejaz, M. Iqbal, A. Anpalagan, and H. S. Kim, "Renewable energy assisted traffic aware cellular base station energy cooperation," *Energies*, vol. 11, no. 1, p. 99, Dec. 2018.
[26] H. A. H. Hassan, A. Pelov, and L. Nuaymi, "Integrating cellular networks, smart grid, and renewable energy: Analysis, architecture, and challenges," *IEEE Access*, vol. 3, pp. 2755–2770, 2015.
[27] A. Jahid, A. S. Ahmad, and M. F. Hossain, "Energy efficient BS cooperation in DPS CoMP based cellular networks with hybrid power supply," in *Proc. 19th Int. Conf. Comput. Inf. Technol. (ICCIT)*, Dec. 2016, pp. 93–98.
[28] K. Huang, M. Kountouris, and V. O. K. Li, "Renewable powered cellular networks: Energy field modeling and network coverage," *IEEE Trans. Wireless Commun.*, vol. 14, no. 8, pp. 4234–4247, Aug. 2015.
[29] H.-J. Hung, T.-Y. Ho, S.-Y. Lee, C.-Y. Yang, and D.-N. Yang, "Relay selection for heterogeneous cellular networks with renewable green energy sources," *IEEE Trans. Mobile Comput.*, vol. 17, no. 3, pp. 661–674, Mar. 2018.
[30] B. Wang, Q. Kong, W. Liu, and L. T. Yang, "On efficient utilization of green energy in heterogeneous cellular networks," *IEEE Syst. J.*, vol. 11, no. 2, pp. 846–857, Jun. 2017.
[31] M. H. Alsharif, "Optimization design and economic analysis of energy management strategy based on photovoltaic/energy storage for heterogeneous cellular networks using the HOMER model," *Solar Energy*, vol. 147, no. 1, pp. 133–150, May 2017.
[32] Y. Zhang, M. Meo, R. Gerboni, and M. Ajmone Marsan, "Minimum cost solar power systems for LTE macro base stations," *Comput. Netw.*, vol. 112, pp. 12–23, Jan. 2017.
[33] A. Aziz, M. Tajuddin, M. Adzman, M. Ramli, and S. Mekhilef, "Energy management and optimization of a PV/Diesel/Battery hybrid energy system using a combined dispatch strategy," *Sustainability*, vol. 11, no. 3, p. 683, Jan. 2019.
[34] A. Abrol and R. K. Jha, "Power optimization in 5G networks: A step towards GrEEn communication," *IEEE Access*, vol. 4, pp. 1355–1374, 2016.
[35] K. Kanwal, G. A. Safdar, M. Ur-Rehman, and X. Yang, "Energy management in LTE networks," *IEEE Access*, vol. 5, pp. 4264–4284, 2017.
[36] H. Ghazzai, E. Yaacoub, A. Kadri, H. Yanikomeroglu, and M.-S. Alouini, "Next-generation environment-aware cellular networks: Modern green techniques and implementation challenges," *IEEE Access*, vol. 4, pp. 5010–5029, 2016.
[37] M. Nahas, M. Ghantous, K. A. H. Ismaiil, and B. Assaf, "For better energy consumption and management in future cellular networks," in *Proc. Int. Conf. Renew. Energies Developing Countries*, Nov. 2014, pp. 127–132.
[38] A. Jahid, A. B. Shams, and M. F. Hossain, "Dynamic point selection CoMP enabled hybrid powered green cellular networks," *Comput. Electr. Eng.*, vol. 72, pp. 1006–1020, Nov. 2018.
[39] M. H. Alsharif, R. Nordin, and M. Ismail, "Energy optimisation of hybrid off-grid system for remote telecommunication base station deployment in malaysia," *EURASIP J. Wireless Commun. Netw.*, vol. 2015, no. 1, pp. 1–15, Mar. 2015.
[40] A. Jahid, A. B. Shams, and M. F. Hossain, "PV-powered CoMP-based green cellular networks with a standby grid supply," *Int. J. Photoenergy*, vol. 2017, Apr. 2017, Art. no. 6189468.
[41] G. Auer, V. Giannini, C. Desset, I. Godor, P. Skillermark, M. Olsson, M. Imran, D. Sabella, M. Gonzalez, O. Blume, and A. Fehske, "How much energy is needed to run a wireless network?" *IEEE Wireless Commun.*, vol. 18, no. 5, pp. 40–49, Oct. 2011.
[42] *Bangladesh Bank Monetary Policy*. Accessed: Nov. 30, 2019. [Online]. Available: https://tradingeconomics.com/country-list/interest rate?continent=asia
[43] *Coordinated multi-point operation for LTE. 3GPP TSG RAN WG1*. 3GPP TR document 36.819 V11.0.0. 2011.
[44] *Bangladesh Energy Regulatory Commission*. Accessed: Nov. 30, 2019. [Online]. Available:http://berc.org.bd

**ABU JAHID** (Student Member, IEEE) received the bachelor's and M.Sc. degrees in electrical engineering from the Military Institute of Science and Technology (MIST), Dhaka, Bangladesh. He is currently pursuing the Ph.D. degree with the Department of Electrical and Computer Engineering, University of Ottawa, Canada. From 2010 to 2012, he worked as a BSS Engineer at Huawei Technologies, where he researches on radio network planning and optimization. He was an Assistant Professor with the Department of EEE, Bangladesh University of Business and Technology, Dhaka, from 2016 to 2019. His research interests include green cellular networking, photonic integrated circuit, and microwave photonics. He has been serving as a TPC member and reviewer in many reputed international journals and conferences.

**MD. SANWAR HOSSAIN** (Student Member, IEEE) received the B.Sc. degree in electrical and electronic engineering (EEE) from the Rajshahi University of Engineering and Technology, Rajshahi, Bangladesh, in 2010. He is currently pursuing the M.Sc. degree in electrical electronic and communication engineering with the Military Institute of Science and Technology (MIST). From 2011 to 2015, he was a Lecturer with the Department of EEE, Bangladesh University of Business and Technology, Dhaka, Bangladesh, where he is currently serving as an Assistant Professor. His research interests include green energy, smart grid, and power system optimization.

**MD. KAMRUL HASAN MONJU** received the B.Sc. degree in electrical engineering from the Bangladesh University of Business and Technology, Dhaka, Bangladesh, in 2017. His current research interests include wireless communications and renewable energy.

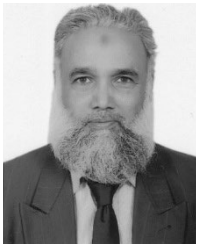

**MD. FAYZUR RAHMAN** was born in Thakurgaon, Bangladesh, in 1960. He received the B.Sc. degree in electrical and electronic engineering from the Rajshahi Engineering College, Bangladesh, in 1984, the M.Tech. degree in industrial electronics from the S. J. College of Engineering, Mysore, India, in 1992, and the Ph.D. degree in energy and environment electromagnetic from Yeungnam University, South Korea, in 2000. He was a Professor in electrical and electronic engineering at the Rajshahi University of Engineering and Technology (RUET) and has served as the HOD for the same department. He has also served as the Departmental Head in the EEE Department, for two years, and in the ETE Department of Daffodil International University, for two years. He is currently a Professor and Chairperson of the IEEE Department of the Green University of Bangladesh. His current research interests are energy and environment electromagnetic, electronics and machine control, as well as high voltage discharge applications. He is a Fellow of the Institution of Engineer's (IEB), Bangladesh, and a Life Member of the Bangladesh Electronic Society.

**MD. FARHAD HOSSAIN** (Member, IEEE) received the B.Sc. and M.Sc. degrees in electrical and electronic engineering from the Bangladesh University of Engineering (EEE) and Technology (BUET), Dhaka, Bangladesh, in 2003 and 2005, respectively, and the Ph.D. degree in electrical and information engineering from The University of Sydney, Australia, in 2014. He currently holds the position of Professor with the Department of EEE. He also works as an Electrical and Electronic Engineering Consultant. He has published over 50 refereed articles in highly prestigious journals and conference proceedings. His research interests include green cellular networks, underwater communications, smart grid communications, sensor networks, network architectures, and protocols designs. He has been serving as a TPC member and reviewer in many international journals and conferences. He was a recipient of the Best Paper Award in three international conferences and the Student Travel Grant in the IEEE Global Communications Conference (GLOBECOM), Anaheim, CA, USA, in 2012.